THE ASTRONOMICAL JOURNAL VOLUME 102, NUMBER 3 SEPTEMBER 1991

THE DISTRIBUTION OF GALAXIES AROUND NGC 5846

M. P. HAYNES
National Astronomy and Ionosphere Center[1] and Center for Radiophysics and Space, Research, Cornell University, Ithaca, New York 14853

R. GIOVANELLI
National Astronomy and Ionosphere Center, Arecibo Observatory, Arecibo, Puerto Rico 00613
Received 9 January 1991; revised 31 March 1991

ABSTRACT

The three-dimensional distribution of galaxies in a region surrounding the chain of galaxies in the NGC 5846 group has been investigated by both subjective and objective tests for clustering. The compilation of a complete redshift sample over the area of study allows the identification of distinct galaxy aggregates and estimation of group properties. Much of the nearby structure, including the NGC 5846 group, is connected into a single prolate cloud of galaxies that points toward the Virgo cluster. Also evident is a tenuous filament of galaxies at a velocity of $\simeq 7000$ km s^{-1} that appears to connect at right angles with an elongated cloud that is identified as the Zw 1400 + 0949 cluster seen in projection. The subconcentration around NGC 5846 is itself a tight, compact configuration, unlike other density enhancements like the Virgo III or Ursa Major Clouds. A comparison of the NGC 5846 group with similar structures in the Local Supercluster confirms the qualitative impression that the highest density environments are dominated by early type systems.

1. INTRODUCTION

The local universe, far from being homogeneous on scales larger than 1 Mpc, is now believed to exhibit large-scale structure in at least two forms: the roughly spherical shells of de Lapparent *et al.* (1986); and the one-dimensional filament that is the main ridge of the Pisces–Perseus supercluster (Giovanelli *et al.* 1986). In fact, the region south of the Pisces–Perseus filament (Haynes & Giovanelli 1986a) contains two-dimensional surfaces similar to those found by de Lapparent *et al.* (1986) in their slice of sky through the galactic pole. The extreme clumping of galaxies on scales of tens of megaparsecs leaves equally large empty "voids" throughout space, a phenomenon first emphasized by observations in the Bootes region by Kirshner *et al.* (1981).

On smaller scales, rich galaxy clusters occupy volumes a few Mpc across, while loose clusters (Zwicky et al. 1961–66, hereafter referred to as CGCG) and smaller groups of galaxies (de Vaucouleurs 1975, hereafter referred to as dV) are 1 Mpc or smaller. Although the rich clusters are believed to be gravitationally bound (though not, in general, virialized), the last two classes of structure are more difficult to analyze both because of their low density enhancement over the background and because of the small number of galaxies—10 to 20—contained within. However, as the membership of such groups becomes possible to determine, it is interesting to investigate the structure of the lower-density galaxy aggregates and to see how they may differ from the richer clusters.

Among the loose groups of galaxies contained within the Local Supercluster but not associated directly with the Virgo cluster, only two are dominated by early type spirals: the groups around NGC 3607 and around NGC 5846 (dV). The central concentration of the latter consists of an arc of bright galaxies quite similar to Markarian's chain in the Virgo cluster. De Vaucouleurs (1960) has pointed out that the group can be relatively well defined as a compact, isolated aggregate, although Tully (1982) using a more extensive dataset has found the group to be a condensation within a loose, prolate cloud that lies about 40 degrees above the plane of the Local Supercluster and points toward the Virgo cluster. Because of the unusual arrangement of galaxies, the dominance by early types and the presence of extended x-ray emission from a central source (Biermann *et al.* 1989), the NGC 5846 region attracted our attention as worth investigating for both its structural and dynamical aspects. The enhancements in the surface density distribution of galaxies at moderate magnitudes in the Serpens–Virgo region are visible in Fig. 2 of Fontanelli (1984). The area of the sky around that occupied by the NGC 5846 group also contains the southern extensions of the A1367/Coma supercluster and the Hercules supercluster (Freudling *et al.* 1988; Freudling 1990) so that a general study of the region around the celestial equator between right ascensions R.A. = 14^h and R.A. = 16^h is desirable.

As part of a preliminary study of this region, we have obtained H I 21 cm line observations of a sample of galaxies in and around the NGC 5846 group. We have combined the new 21 cm observations with other available redshifts and H I data for a region of sky which contains the NGC 5846 and Virgo III groups of dV and the nearby CGCG cluster Zw 1400 + 0949 in order to perform both subjective and objective clustering analysis on the position-redshift data. In Sec. 2, we define the region and describe the H I observations and other data. Section 3 describes the search for true three-dimensional structure. The properties of these groupings including the morphological and properties of their constituent members are analyzed in Sec. 4. The last section contains a summary of our conclusions.

2. OBSERVATIONS AND SAMPLE DEFINITION

Initially, this investigation was directed toward the mapping of the membership of the galaxy group dominated by NGC 5846. The group around NGC 5846 has an observed mean recessional velocity of about 1900 km s^{-1}. In order to

[1] The National Astronomy and Ionosphere Center is operated by Cornell University under a management agreement with the National Science Foundation.

 0004-6256/91/030841-23$00.90

examine the group immediately surrounding NGC 5846 as well as its possible connection with other hierarchical structures, the region of study was originally extended to cover from 14^h to 16^h right ascension, and from $-5°$ to $+12°$ declination. Because of the presence of structure located close to the western boundary at R.A. = 14^h, the region was later extended westward to R.A. = 13^h45^m. This area of sky encompasses the groups designated in dV's list as G29 (the Virgo III cloud) and G50 (the NGC 5846 group), as well as the loose CGCG cluster Zw 1400 + 0949, sometimes called the NGC 5416 cluster (Thompson *et al.* 1979) or group (Chincarini *et al.* 1979). The southern boundary is somewhat arbitrary, and is set by the existence of new H I data as far south as -5 degrees. Although the CGCG fields extend down to -3.5 degrees, the redshift data become rapidly incomplete south of -2.5 degrees, where the cataloguing by Nilson (1973, hereafter referred to as UGC) cuts off. The possibility of structure extending to the south is discussed below. The area studied is about 1% of the entire sky.

As an introduction to the region, Fig. 1 shows the sky distribution of several samples of galaxies relevant to our study. In the bottom panel, the locations of all 1729 CGCG galaxies in the field are plotted. Open circles denote galaxies of magnitude + 14.9 and brighter while open triangles mark the fainter objects. In the middle panel, the open circles show only the brighter set of galaxies. In the top panel, asterisks indicate the sky distribution of all 553 galaxies with measured redshifts $V_\odot < 12\,000$ km s^{-1} and magnitudes of 15.7 and brighter. In the following, we shall combine redshifts with the positional data to investigate the three-dimensional structure in and around NGC 5846.

2.1 New 21 cm Observations

As part of the study of this region, we have obtained new 21 cm line spectra of 94 spiral galaxies for which H I data were not previously available. 81 of the galaxies were observed with the dual circular feed system of the Arecibo 305 m telescope using the standard observational technique described in Haynes & Giovanelli (1984). The 21 cm line spectra thus obtained at Arecibo are shown in Fig. 2. For 13 objects lying south of the Arecibo declination limit (Dec. $< -1°$), and for 3 galaxies (UGC 9215, 9462, and 9794) whose optical angular sizes suggested inadequate coverage with a single Arecibo beam (HPBW = 3.3 arcmin), H I line spectra were obtained with the late 91 m telescope (HPBW = 10 arcmin) of the National Radio Astronomy Observatory.[2] The observational setup and method has been described by Haynes *et al.* (1988). The H I spectra obtained with the 91 m telescope are shown in Fig. 3.

Previous experience (e.g. Hewitt *et al.* 1983) has shown that with proper calibration, integrated line fluxes measured with both telescopes are accurate to about 15% after correction for gain variations and geometry. Observations conducted with the 305 m telescope had slightly higher spectral resolution, about 15 km s^{-1}, compared with about 22 km s^{-1} for those using the 91 m. At both telescopes, initial observations were conducted in a standard search mode in which the autocorrelator was configured as four separate quadrants, each covering 10 MHz and offset 7.5 MHz in frequency. After detection, a second set of spectra were obtained with the 91 m telescope switching its correlator configuration in order to achieve adequate resolution. In all cases, a total power beam-switching (ON–OFF) observing technique was employed. The spectra displayed in Figs. 2 and 3 are the final ones resulting after the calibration, accumulation and averaging of a number of individual ON–OFF pairs, and have been hanning smoothed. The noiseless curve superimposed on each spectrum is the polynomial baseline removed from the profile before moment measurements were made.

Table 1 presents the results of the 21 cm line observations shown graphically in Figs. 2 and 3. For each entry, the following information is listed:

Column (1). Field and sequential entry number (per field) in the CGCG.

Column (2), line 1. Entry number in UGC; line 2: Entry number in NGC or IC or alternative name.

Column (3). Right ascension in hhmmss.s format (line 1) and declination in sddmmss format (line 2). Positions have been taken from Dressel & Condon (1976) or measured from the Palomary Sky Survey (PSS) using a standard overlay technique.

Column (4). Morphological type code used, based on the system used by deVaucouleurs *et al.* (1976).

Column (5), line 1. Blue major and minor diameters a and b, in arcminutes, from the UGC were available. For galaxies not included in the UGC, a and b were estimated from glass copies of the PSS or from a film copy of the UK–Schmidt J print. Line 2: Inclination i in degrees, estimated from the axial ratio and an assumed type-dependent intrinsic axial ratio, following Haynes & Giovanelli (1984).

Column (6), line 1. Magnitude m, on the CGCG scale, either from the CGCG or the UGC; line 2: Corrected magnitude m_c, after consideration of systematic effects, redshift and galactic and internal extinction corrections following Haynes & Giovanelli (1984). Systematic effects are uncertain for objects fainter than $m = 15.4$ in Volume I of the CGCG.

Column (7), line 1. Heliocentric radial velocity $V_\odot$, in km s^{-1}, measured as the midpoint of the H I profile at a level of 50% of the mean signal intensity; line 2: Hubble velocity V_H, in km s^{-1}. Heliocentric velocities were corrected with respect to the Local Group to V_{LG} by addition of the standard 300 sin l cos b km s^{-1} term. The conversion to a Hubble velocity used two different methods, depending on the value of V_{LG}. When $V_{LG} < +3000$ km s^{-1}, we assumed that the galaxy was a member of, or at least stationary with respect to the Local Supercluster; this cutoff was determined by looking at position-velocity cone diagrams and was fairly unambiguous (see Sec. *3.1*). The velocities of such objects were corrected for Local Group infall of magnitude 300 km s^{-1} toward the center of the Virgo Cluster. Galaxies with V_{LG} greater than +3000 km s^{-1}, on the other hand, were assumed to be stationary with respect to the cosmic microwave background (CMB). We used the Lubin *et al.* (1985) result for solar motion with respect to the CMB. When referred to the Local Group barycenter, this correction amounts to 620 km s^{-1} toward R.A. = 10^h30^m, Dec. = $-25°$, or $l = 267°$, $b = +28°$. We regard these corrections only as a best attempt for the present, given the probability of large-scale peculiar velocities in the local universe (Faber & Burstein 1988).

Column (8), line 1. Observed H I line flux, S_0, in Jy km s^{-1}; line 2: Corrected H I line flux S_c in Jy km s^{-1}.

[2] The National Radio Astronomy Observatory is operated by Associated Universities Inc. under contract from the National Science Foundation.

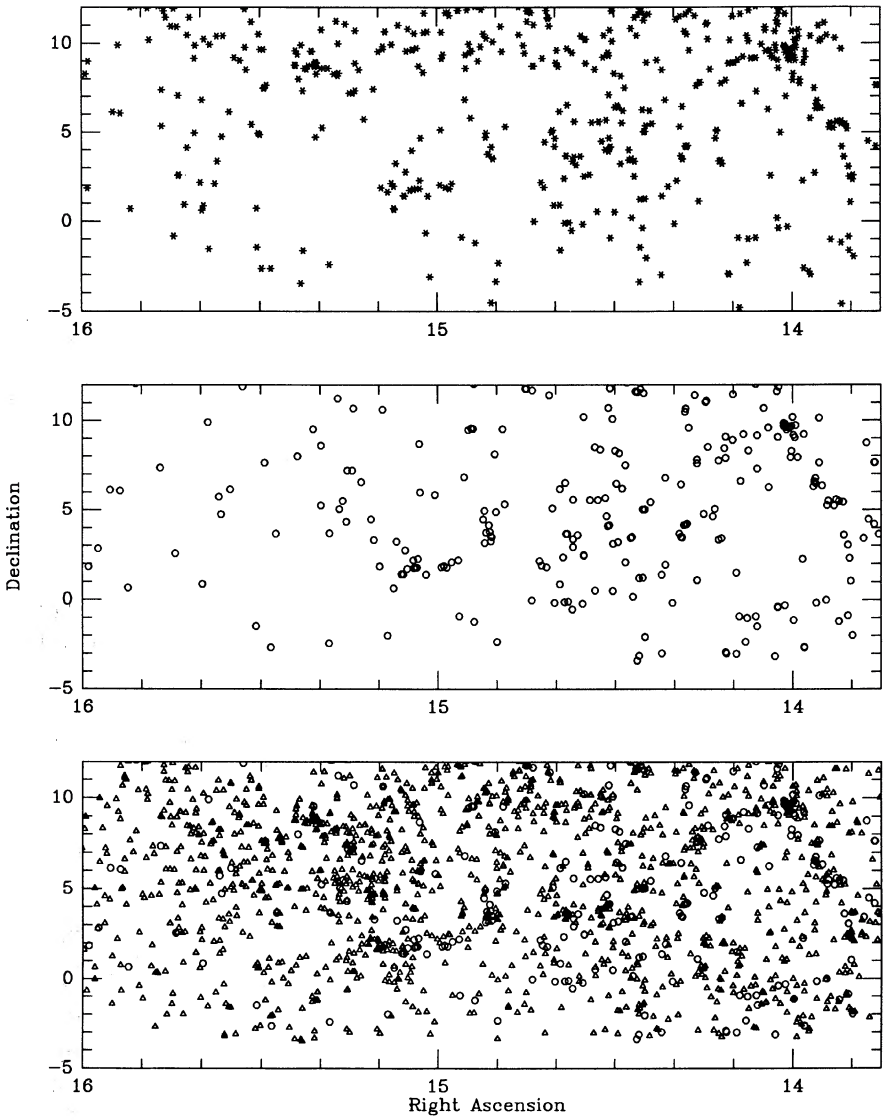

FIG. 1. Sky distribution of galaxies in the region of study. The upper panel shows the distribution of the 582 galaxies with measured redshifts. The middle panel shows the 225 galaxies in the CGCG redshift sample with $V_H < 12\,000$ km s^{-1} and $m \leqslant 14.9$. The bottom panel includes all CGCG in the region covered by that catalog. Galaxies denoted by a triangle are fainter than $m = 14.9$; open circles mark brighter objects.

Corrections for resolution and internal absorption as discussed by Haynes & Giovanelli (1984) have been applied.

Column (9). rms noise in mJy of smoothed, baselined H I spectrum.

Column (10). Observed 21 cm line width W, in km s^{-1}, measured as the full-width at a level of 50% of the mean signal intensity; line 2: Corrected 21 cm line width W_0, in km s^{-1}, after accounting for redshift and inclination. W_0 is given only for galaxies with inclinations larger than 30°.

Column (11), line 1. Telescope code indicating which telescope was used for the observations. "*G*" refers to the Green Bank 91 m; "*c*" refers to the Arecibo dual circular feed. A few objects were observed with both instruments. Line 2 contains a subjective index of the H I profile quality: (1) good detection; (2) marginal detection, parameters uncertain; and (3) velocity and flux probably acceptable, but width measurement uncertain.

Where necessary, comments on the H I observations and spectra for individual objects are presented in the notes to Table 1. These data have been combined with others from the literature to construct samples for the study of galaxy properties in this region. In the next section, we outline the various subsamples that we have compiled for further analysis.

2.2 Sample Definition

Within this region, redshifts are available for a total of 582 galaxies. For galaxies for which H I observations were not made by us, redshifts were taken from compilations such as that of Palumbo *et al.* (1983), a private one kindly provided by J. Huchra in early 1989, and our own database. Binning this "redshift sample" by CGCG magnitude shows that it becomes sharply incomplete fainter than magnitude + 14.9, whereas a similar analysis of all CGCG galaxies in this region shows completeness down to + 15.3, as is the case with the CGCG as a whole (e.g., Giovanelli & Haynes 1982). We

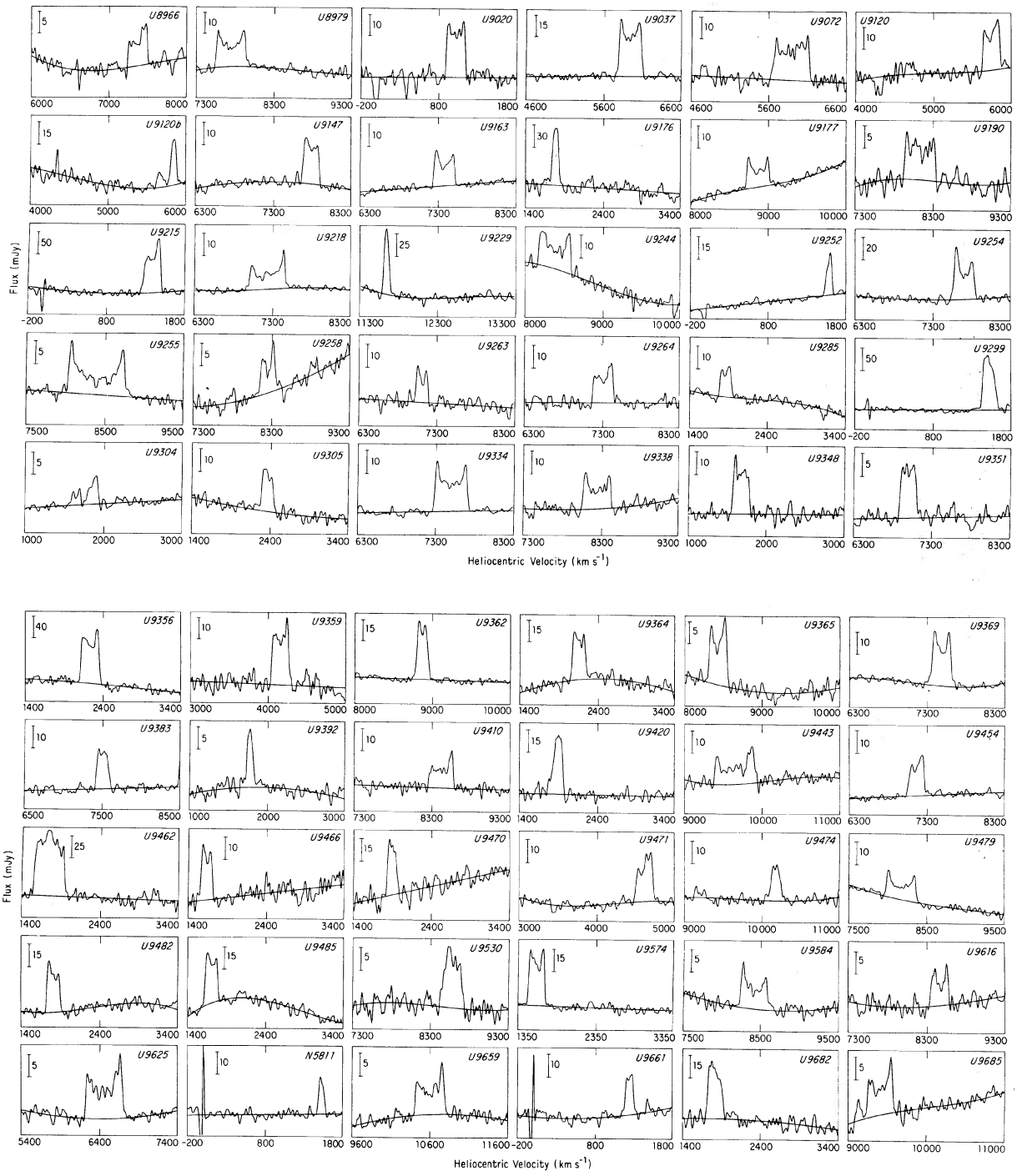

FIG. 2. H I line spectra of galaxies observed with the Arecibo 305 m telescope. The superimposed noiseless curve shows the polynomial baseline that was subtracted.

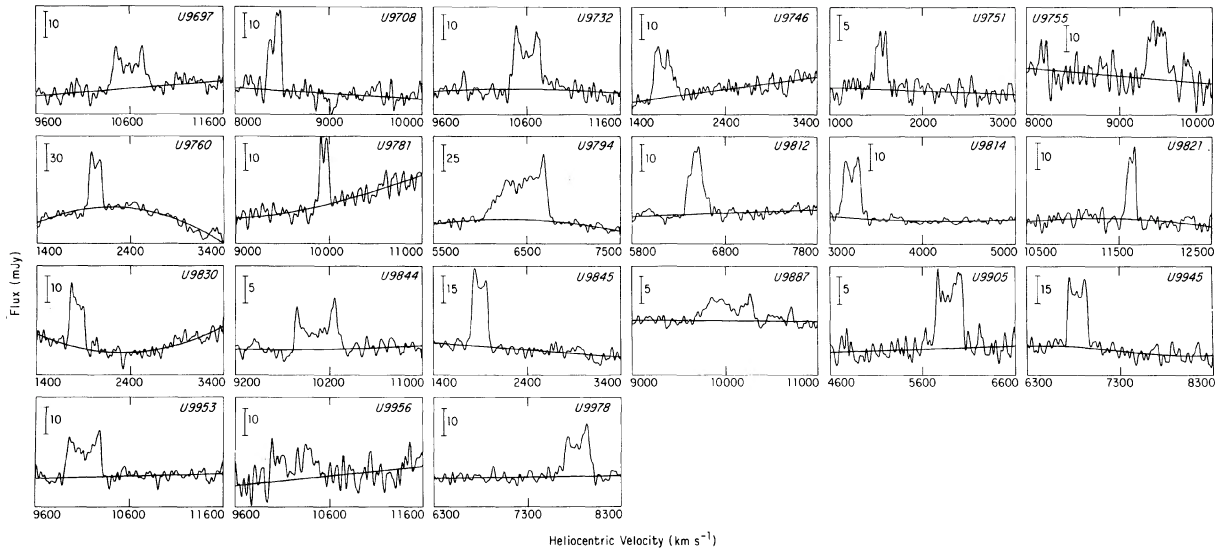

FIG. 2. (continued)

therefore also define a "restricted redshift sample" of the 225 objects with magnitudes + 14.9 and brighter.

Figure 4(a) shows the distribution of recessional velocities V_H for the restricted redshift sample compared with that which one would expect for a homogeneous distribution. Note that we adopt $H_0 = 100$ km s^{-1} Mpc^{-1} throughout this paper, and no corrections for local peculiar motions have been applied. Shown as the smooth curved superimposed on the histogram, the predicted distribution has been derived from a Schechter (1976) luminosity function, fit to our redshift catalog with the same apparent magnitude limit imposed and confined to the regions ($b > 40°$, Dec. $> +0°$) and ($b < -30°$, Dec. $> -2.5°$). Galaxies within six degrees of the center of the Virgo cluster were excluded. The parameters for the best-fit Schechter function are $\alpha = -1.45$, $M^* - 19.4$, and normalization constant 0.0085 Mpc^3 mag^{-1}. The normalization was fit, and was not set such that the areas under the observed and predicted curves in Fig. 4(a) would be equal. The fact that this equality does indeed approximately hold upon integration indicates that the restricted sample is truly complete to the stated magnitude limit. However, the assumption of homogeneity is obviously incorrect: the galaxies are strongly clumped around 2000 and 7000 km s^{-1}, with a large underdense region in between. These enhancements reflect the structure associated with the Local Supercluster and the Zw 1400 + 0949 group, respectively.

Based on the low number of expected objects beyond 12 000, we set an arbitrary cutoff at the corresponding value of the Hubble velocity $V_H = 12\,000$ km s^{-1}. While this cutoff excludes no objects from the restricted redshift sample, establishing such a limit is necessary for the percolation analysis used in Sec. *3.2*. In Fig. 4(b), we show the observed distribution of velocities for all 553 galaxies which are closer than $V_H = 12\,000$ km s^{-1}, regardless of magnitude. This plot shows that, while it is possible that deeper redshift surveys will "fill in" the void at $\simeq 3000$ km s^{-1}, all current evidence points to a significant underdensity at that distance. In fact, inspection of cone diagrams covering a much larger area indicates that this mostly empty region can be considered a continuation of the void which lies behind the Virgo cluster and in front of the Coma cluster. In both panels of Fig. 4, we see evidence for enhanced populations in three separate redshift regimes: the excess at ($V_H \leqslant 3000$ km s^{-1}), identified with the Local Supercluster; the peak at $V_H \simeq 7000$ km s^{-1} that encompasses the Zw 1400 + 0949 cluster and may connect to the Coma/A1367 supercluster, and additional objects with $V_H > 8000$ km s^{-1}. At the higher redshifts, the southern extension of the Hercules supercluster makes a considerable contribution, despite its greater distance and the current survey incompleteness. In the subsequent analysis, we will attempt to clarify the location and significance of the apparent structures.

In addition to the observations reported in Sec. *2.1* and good quality H I profiles reported in the literature, we obtained unpublished 21 cm data from an unrelated project of ours (Haynes *et al.* 1991), and especially from an ongoing H I survey of the Hercules supercluster region (Freudling *et al.* 1989; Freudling 1990). Because a number of the nearby objects have angular sizes that are large relative to the dual circular feed beam, we have used, where available, large-beam observations for unconfused galaxies with UGC diameters larger than 3.0 arcmin in preference to Arecibo data. In all, 357 objects have H I detections or restrictive upper limits, 350 of them closer than our redshift cutoff. Of these galaxies, 310 have morphological types from Sab to Irr (i.e., are not early, peculiar, or unclassifiable). These 310 late-type objects constitute our "H I sample". Most (289) of these galaxies are bright enough to be included in the CGCG, but only about half (123) would pass the magnitude cutoff of 14.9 imposed on the complete redshift sample described earlier.

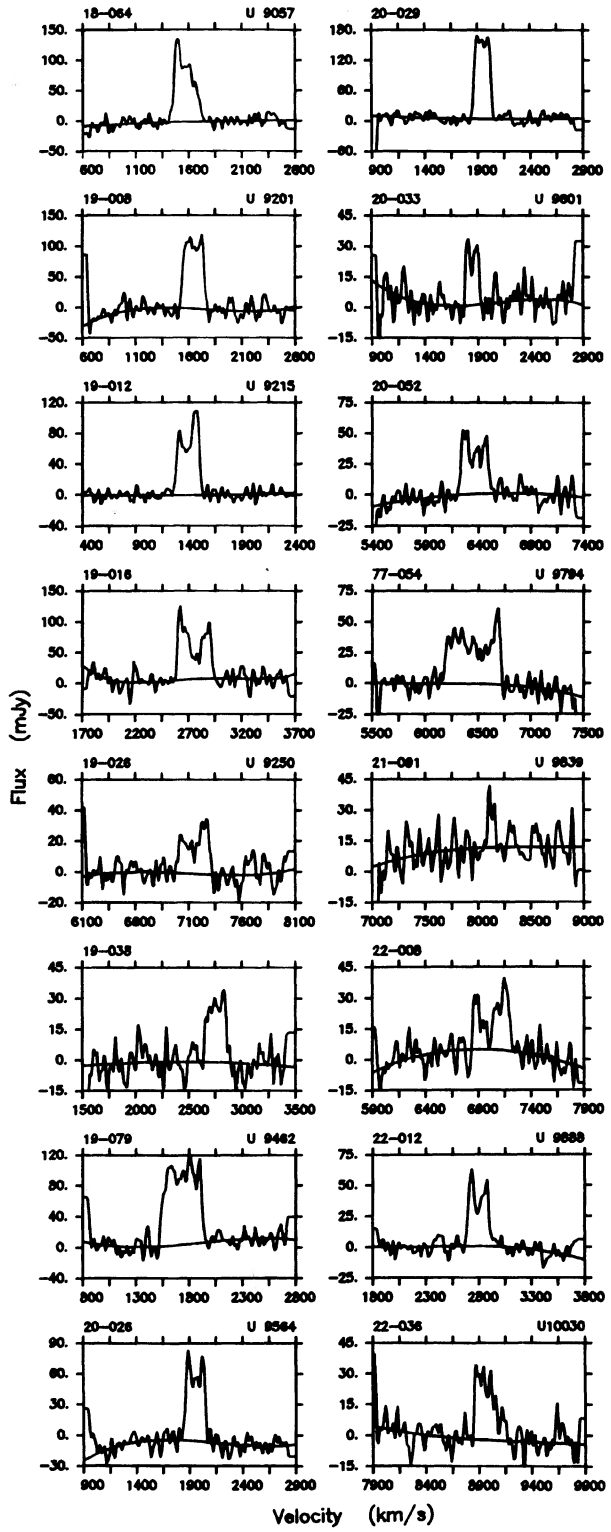

FIG. 3. Same as Fig. 2 for the galaxies observed with the Green Bank 91 m telescope.

3. IDENTIFICATION OF STRUCTURE

3.1 Visual Inspection

An examination of various displays of the three-dimensional coordinates available for galaxies in this region gives a subjective impression of the structure. In practice, this visual inspection was performed in advance of any quantitative analysis, but here, we shall make use of our results to clarify the presentation. Both to aid the reader at this point and to quantify results derived in the next section, Table 2 summarizes the properties of the major three-dimensional features. For the moment, the mean 3D locations ($\langle$R.A.$\rangle$, $\langle$Dec.$\rangle$, $\langle V_H \rangle$) of the 11 most prominent groups, whose identification will be examined later, are to be used only to guide the reader as we perform the visual inspection of the redshift catalog. For clarification purposes, Fig. 5 shows the sky location of the 11 groups. Because the groups cannot be characterized in any simple manner, we show them first by displaying in the lower panel their constituent membership, plotting each galaxy separately. In the upper panel, the mean sky position of each group is noted. Different symbols denote objects in the three redshift regimes that are evident in Fig. 4. The Local Supercluster groups ($V_H \leqslant 3000$ km s^{-1}) are shown by circles while the two features with $\langle V_H \rangle \sim 7000$ km s^{-1} are marked with triangles. The most distant objects with $V_H > 8000$ km s^{-1} are shown by asterisks. In order that distinction be made between adjacent groups in the same redshift range, some symbols are filled and some are open, but this distinction is purely for the convenience of illustration. The reader should keep in mind that the redshift catalog is complete only for the nearest objects and that, in particular, serious incompleteness limits our understanding of the most distant objects.

A first note about nomenclature must be made for clarification purposes. Because different criteria and catalogs of different depths are used by various authors (including ourselves) in identifying groups of galaxies, confusion sometimes results. We identify in Table 2 the names associated with the groups used in the remainder of this paper with those used by other authors to refer to the same features. Referring back to Fig. 4, we can identify the nearby population of galaxies with at least 5 distinct groups. Two of these are the Virgo III cloud and the NGC 5846 group, as mentioned before, identified by dV. Two of the remaining three are included in the catalog of groups constructed by Geller & Huchra (1983, hereafter referred to as GH) from the Center for Astrophysics survey. We retain the group numbering from GH and refer to these groups as CfA 139 and CfA 148. The final nearby group is now evident because of the increased depth of the current redshift catalog and is identified by its brightest member NGC 5718. More distant groups are also denoted by their brightest members, except in the case of the diffuse and elongated "filament" which, as described below, includes the Zw 1400 + 0949 cluster. As noted in Table 2, several groups can be identified with structures known by other names.

The next several figures serve to summarize our visual impression of the region. As a refinement to Fig. 4, in Fig. 6 the region is divided by right ascension into four unequal segments: two narrow strips covering the Zw 1400 + 0949 and NGC 5846 groups, respectively, and two wider strips which together cover the rest of the area. The choice of these boundaries has been made to emphasize the structures seen in this region. Figures 6(a)–6(d) display the velocity distributions for the four regions, ordered in an easterly direction. Both the entire redshift sample (single hatched area) and the restricted redshift sample (cross hatched area) are included. In Fig. 6(a) which extends from $13^h52^m <$ R.A. $< 14^h07^m$ and covers the Zw 1400 + 0949 cluster, all of the

TABLE 1. Properties of observed galaxies.

CGCG	UGC NGC	RA Dec.	T	a x b i	m_z m_c	V_o V_H	S_{obs} S_c	rms	W W_c	Tel. Qual
046-043	8966	140100.0	7	1.1x 0.6	15.3	7379	1.86	2.1	262	c
		+070100		60	15.2	7653	2.27		303	1
046-044	8979	140133.7	6	1.3x 0.1	16.0	7436	4.68	1.5	385	c
		+064320		90	14.7	7709	7.44		385	1
046-050	9020	140401.7	5	2.6x 0.4	14.5	5938	9.09	1.5	302	c
	N5470	+061601		90	13.3	6209	15.83		302	1
046-060	9037	140600.1	7	1.8x 0.9	14.5	5940	8.77	1.9	301	c
		+071743		60	13.9	6208	11.68		349	1
018-064	9057	140737.6	8B	3.0x 1.0	14.4	1573	22.62	9.1	248	G
		-022017		71	13.5	1773	27.92		262	3
046-063	9072	140827.7	5	1.6x 1.0	13.9	5886	6.79	2.5	470	c
	N5491	+063601		51	13.2	6152	8.72		601	1
046-075	9120	141242.0	7	1.1x 0.8	14.6	5746	5.00	2.5	232	c
		+050323		43	14.2	6009	5.88		339	1
018-114	9147	141542.0	6	1.6x 1.0	14.9	7789	3.66	1.4	212	c
	I 942	+010700		51	14.6	8052	4.66		272	1
075-007	9163	141625.2	7	1.3x 0.3	15.6	7373	3.10	1.0	278	c
		+113100		77	15.3	7623	4.24		285	1
047-013	9176	141800.4	7	2.0x 1.6	14.9	1773	6.77	6.6	107	c
	N5569	+041240		37	14.8	2008	9.21		178	1
075-014	9177	141804.6	7	1.4x 1.2	14.9	8860	2.68	1.1	297	c
		+103926		31	14.8	9109	3.26		574	1
047-024	9190	141859.2	5	1.3x 0.5	15.3	8126	2.59	1.5	396	c
		+051800		69	15.0	8381	3.38		425	1
019-008	9201	141949.9	7	3.5x 2.8	12.8	1641	22.44	14.3	209	G
	N5584	-000934		37	12.1	1855	25.13		346	1
019-012	9215	142054.5	7B	2.5x 1.3	13.6	1392	19.42	4.7	223	c,G
		+015701		58	12.8	1617	29.00		262	1
047-030	9218	142121.6	5	1.5x 0.6	14.7	7221	3.55	1.1	460	c
	N5599	+064800		68	14.1	7471	4.72		497	1
019-017	9229	142158.4	5	1.0x 0.9	14.9	11642	5.05	3.1	86	c
		+012420		26	14.7	11897	5.77			1
019-016		142205.9	5	2.0x 0.9	13.8	2743	21.70	14.6	325	G
	N5604	-025855		64	12.9	2943	25.03		361	1
047-038	9244	142338.2	7B	1.3x 0.7	14.8	8374	4.41	1.4	420	c
		+052740		57	14.4	8623	5.46		502	1
019-026	9250	142435.8	7B	1.8x 1.2	14.8	7158	7.10	6.8	303	G
	N5618	-020256		48	14.4	7412	7.65		409	1
047-042	9252	142440.6	9	1.1x 0.2	15.7	1585	1.98	1.3	99	c
		+052120		81	15.7	1827	2.18		101	1

TABLE 1. (continued)

CGCG	UGC NGC	RA Dec.	T	a x b i	m_z m_c	V_o V_H	S_{obs} S_c	rms	W W_c	Tel. Qual
019-028	9254	142446.7	5B	2.3x 2.2	14.8	7697	8.09	2.1	270	c
	I1010	+011453		17	14.6	7949	11.97			1
047-044	9255	142447.6	5	2.4x 1.1	14.0	8384	3.85	0.7	727	c
	N5619	+050135		64	13.2	8632	5.74		812	1
047-047	9258	142459.5	5	1.0x 0.9	15.3	8249	1.33	1.5	196	c
		+050007		26	15.3	8497	1.52			1
019-032	9263	142510.7	8	1.1x 0.9	15.6	7104	1.90	2.1	160	c
		-002253		35	15.6	7356	2.15		277	1
047-051	9264	142510.2	7	1.0x 0.2	15.5	7314	3.13	2.7	278	c
		+061543		79	15.0	7560	4.26		283	1
019-038		142547.9	7	1.3x 1.1	14.6	2755	5.86	6.8	211	G
		-032257		32	14.3	2954	6.07		394	1
047-058	9285	142632.2	7	1.3x 0.3	15.3	1860	1.75	1.5	166	c
		+032200		77	14.8	2093	2.39		170	1
019-044	9299	142700.9	7	1.7x 0.9	14.7	1531	18.68	3.4	190	c
		+001200		58	14.2	1749	24.42		225	1
047-062	9304	142707.8	3B	1.5x 1.1	14.6	1664	1.03	0.6	356:	c
	N5636	+032920		44	14.3	1898	1.24		514:	2
	9305	142710.0	8	1.1x 0.2	16.0	2366	2.60	1.8	158	c
		+041707		81	15.2	2604	2.86		160	1
047-072	9334	142831.5	6B	2.1x 1.5	13.8	7496	9.57	1.3	426	c
	N5652	+061158		44	13.2	7738	13.25		609	1
047-073	9338	142842.5	7	1.1x 0.4	15.2	8235	3.84	1.7	374	c
		+053137		72	14.6	8478	4.86		402	1
019-057	9348	142955.3	5	1.8x 0.3	14.6	1673	4.04	2.4	224	c
		+003047		90	13.4	1893	6.28		224	1
	9351	143002.7	9	1.1x 0.1	17.0	6997	2.31	1.4	219	c
		+055320		90	15.7	7238	3.70		219	1
075-065	9356	143028.4	5	1.6x 0.8	14.3	2228	18.88	4.8	249	c
		+114851		61	13.7	2500	24.74		286	1
019-060	9359	143039.8	9	1.5x 0.2	15.6	4153	5.04	2.8	226	c
		-005500		90	14.7	4399	8.23		226	1
047-088	9362	143046.2	6	1.1x 1.0	14.9	8869	5.26	1.3	161	c
		+040713		25	14.8	9111	6.08			1
047-091	9364	143051.8	8B	1.8x 0.8	15.0	2153	5.09	3.3	183	c
		+070534		65	14.6	2405	6.94		202	1
047-093	9365	143059.1	6	1.1x 0.9	15.0	8428	2.64	1.3	237	c
		+035427		35	14.9	8669	3.08		409	1
047-096	9369	143122.3	6B	1.2x 1.1	13.7	7477	5.07	0.9	261	c
	N5674	+054043		24	13.1	7716	5.95			1

TABLE 1. (continued)

CGCG	UGC NGC	RA Dec.	T	a x b i	m_z m_c	V_o V_H	S_{obs} S_c	rms	W W_c	Tel. Qual
047-110	9383	143238.7	5	1.1x 0.6	14.2	7500	2.64	1.3	178	c
	N5679	+053440		57	13.5	7738	3.23		211	1
	9392	143315.8	9	1.4x 0.2	17.0	1773	1.08	1.0	107	c
		+031534		90	15.9	2007	1.65		107	1
075-092	9410	143446.4	6	1.4x 0.4	15.3	8420	3.03	1.7	317	c
		+085134		75	14.9	8651	4.07		329	1
019-070	9420	143519.6	5B	1.9x 1.6	12.9	1873	5.19	2.4	158	c
	N5691	-001053		33	12.2	2091	6.95		288	1
075-103	9443	143704.7	2	1.5x 0.5	15.4	9660	6.75	3.0	530	c
		+092647		75	15.4	7.73	9887		550	1
047-122	9454	143754.5	7B	1.4x 1.1	14.9	7148	3.00	2.0	191	c
		+063107		38	14.7	7378	3.66		308	1
019-079	9462	143822.8	5	3.2x 1.2	13.8	1730	35.36	8.8	391	c,G
	N5719	-000615		69	12.8	1948	43.13		417	1
019-080	9466	143826.0	7B	1.1x 0.8	14.5	1631	3.20	3.2	157	c
	N5725	+022401		43	14.0	1862	3.76		230	1
019-082	9470	143915.1	8B	1.2x 0.7	14.9	1894	4.15	4.5	133	c
		+005401		55	14.5	2118	5.09		163	1
047-134	9471	143914.2	5B	1.2x 0.5	14.9	4607	3.79	1.5	234	c
		+060947		66	14.4	4836	4.85		256	3
075-113	9474	143930.1	7	1.1x 0.9	15.0	10178	3.03	1.8	159	c
		+084020		35	14.9	10403	3.53		274	1
047-138	9479	144002.2	5	1.5x 0.5	15.2	8166	3.02	1.1	389	c
		+043834		72	14.7	8395	4.11		409	1
020-003	9482	144013.5	7	1.2x 0.2	15.4	1802	4.64	2.4	182	c
		+005226		85	14.6	2026	6.83		183	1
048-007	9485	144032.9	8	1.6x 0.4	15.4	1698	4.80	2.5	174	c
		+045847		76	14.9	1942	6.88		177	5
076-051	9530	144515.3	7	1.0x 0.7	15.0	8580	2.81	1.7	253	c
		+095157		45	14.8	8796	3.28		356	3
020-026	9564	144932.3	7	2.0x 1.7	14.2	1955	13.41	6.8	203	G
	N5768	-021927		32	13.6	2164	14.12		383	1
020-029		144959.9	8B	2.8x 2.2	15.2	1950	25.32	8.4	172	G
	UA396	-032056		38	15.2	2154	26.68		276	1
048-050	9574	145034.5	5B	2.2x 1.7	13.6	1577	6.64	1.9	215	c
	I1067	+033206		40	12.9	1815	9.44		334	1
048-066	9584	145146.2	5	1.1x 0.4	15.3	8410	2.06	1.0	356	c
		+044247		70	14.9	8623	2.66		378	1
020-033	9601	145330.2	8B	1.5x 1.4	14.6	1851	3.47	6.3	139	G
		-011155		21	14.2	2066	3.57			1

TABLE 1. (continued)

CGCG	UGC NGC	RA Dec.	T	a x b i	m_z m_c	V_o V_H	S_{obs} S_c	rms	W W_c	Tel. Qual
076-104	9616	145426.8	3	1.1x 0.9	14.8	8453	1.42	1.3	237	c
		+092813		36	14.6	8657	1.62		402	1
048-077	9625	145516.6	4B	1.7x 0.5	14.7	6459	3.79	1.1	480	c
		+064926		76	14.0	6665	4.88		494	1
020-043		145755.2	9	0.9x 0.6	14.8	1527	1.16	1.6	99	c
	N5811	+014912		52	14.6	1758	1.27		127	1
048-090	9659	145919.5	7	1.0x 0.3	15.3	10600	2.41	2.4	383	c
		+050740		70	14.9	10803	3.04		409	1
020-048	9661	145930.9	8B	1.4x 1.3	15.0	1240	1.96	1.6	124	c
		+020214		22	14.9	1472	2.38			1
020-052		150111.8	7	2.2x 1.8	15.2	6367	10.29	7.0	271	G
		-030604		35	15.2	6573	10.95		469	1
020-055	9682	150155.3	8	1.9x 0.6	15.3	1823	6.21	3.2	207	c
		-003933		72	14.8	2042	8.93		218	1
048-103	9685	150218.0	7	1.0x 0.8	15.1	9407	1.73	1.0	329	c
		+082200		37	15.1	9602	1.99		545	1
	9697	150312.4	9	1.1x 0.4	16.0	10604	3.91	1.9	392	c
		-003120		69	15.3	10806	5.05		421	1
076-153	9708	150406.0	7	1.1x 1.0	15.2	8424	2.57	3.0	160	c
		+093800		25	15.2	8615	2.97			3
021-014	9732	150536.9	5B	1.3x 0.7	14.7	10600	5.00	2.4	298	c
		+012627		58	14.1	10797	6.26		353	1
021-028	9746	150744.4	6	1.4x 0.3	15.0	1748	3.48	2.1	256	c
		+020727		80	14.3	1981	4.85		261	3
021-032	9751	150825.3	7	1.1x 0.2	15.6	1552	1.28	1.4	150	c
		+013747		90	14.6	1783	1.77		151	3
077-021	9755	150848.5	7	1.1x 0.9	14.8	9024	4.44	2.1	227	c
		+103820		35	14.6	9207	5.17		393	1
021-041	9760	150930.0	7	2.8x 0.2	14.9	2023	7.76	4.6	158	c
		+015200		90	13.5	2255	14.90		158	1
049-072	9781	151220.7	6	1.4x 1.4	15.7	9947	2.32	2.2	116	c
		+054357		0	15.7	10131	2.81			1
077-054	9794	151346.7	8B	3.0x 0.8	14.3	6451	18.61	6.5	528	c,G
		+104133		75	13.4	6627	19.36		546	1
077-071	9812	151641.6	7	1.0x 0.2	15.5	6404	3.96	1.4	210	c
		+095826		83	14.9	6577	5.60		212	3
077-073	9814	151701.8	8	1.1x 0.4	14.7	3231	3.23	1.4	210	c
		+111400		70	14.5	3404	3.57		223	1
077-084	9821	151913.0	5B	1.5x 1.5	15.1	11562	1.66	2.0	89	c
		+083540		0	14.9	11733	2.04			1

TABLE 1. (continued)

CGCG	UGC NGC	RA Dec.	T	a x b i	m_z m_c	V_o V_H	S_{obs} S_c	rms	W W_c	Tel. Qual
049-152	9830	152031.3	7	1.5x 0.2	15.5	1827	3.03	2.0	182	c
		+044220		85	14.8	2073	4.55		183	1
021-091	9839	152241.9	5	1.0x 0.2	15.4	8130	1.67	7.4	83	G
		-013857		83	14.5	8305	2.16		83	2
049-168	9844	152325.5	5B	1.6x 0.6	14.8	10084	2.33	1.0	493	c
		+075947		72	14.1	10249	3.19		520	1
077-127	9845	152340.6	7	1.6x 0.2	15.3	1894	6.61	1.3	183	c
		+092246		90	14.3	2161	10.52		183	1
022-008		152942.0	7	1.3x 0.8	15.7	7028	6.71	6.0	361	G
		-023856		54	15.7	7193	7.29		445	1
050-031	9887	153014.7	5	1.3x 0.4	15.1	10003	2.18	0.7	595	c
		+045500		74	14.5	10161	2.94		618	3
022-012	9888	153030.5	5	1.7x 1.0	14.5	2797	9.49	4.9	220	G
	I1125	-012740		54	13.7	3012	10.46		271	1
078-014	9905	153216.5	7	1.0x 0.1	15.6	5882	3.48	1.5	311	c
		+083000		89	14.7	6034	5.20		311	1
050-066	9945	153624.9	7	1.3x 1.2	14.4	6841	7.25	3.3	236	c
		+044443		23	14.0	6990	8.64			1
050-073	9953	153708.2	7B	1.4x 0.9	15.0	10106	4.38	1.7	383	c
		+032147		49	14.7	10255	5.41		504	1
078-040	9956	153715.3	5	1.0x 0.2	15.4	10248	1.19	0.7	498	c
		+102300		83	14.7	10390	1.67		501	2
050-084	9978	153944.2	7	1.3x 0.5	15.2	7836	3.91	1.4	287	c
		+064820		67	14.8	7978	5.02		312	1
022-036	10030	154429.9	4B	1.4x 0.8	15.4	9000	6.74	5.4	291	G
		-004957		56	15.1	9141	7.11		352	3

Notes to TABLE 1

U 8966 – asymmetric profile.

U 9120 – possibly confused. U 9120 is the brightest of 4 spirals. A second spectrum, labelled U 9120b was obtained three minutes to the north of U 9120, at the position of CGCG galaxy 046-076. This Sc object is 0.9x0.9' in size, at a separation of 2.9 arcmin. It may be responsible for the narrow feature seen in the spectrum marked U 9120b.

U 9304 – aymmetric profile.

U 9462 – emission resolved by Arecibo beam. Parameters derived from 91m telescope observations.

U 9839 – low signal to noise.

U 9887 – width not well–defined.

U 9956 – low signal to noise.

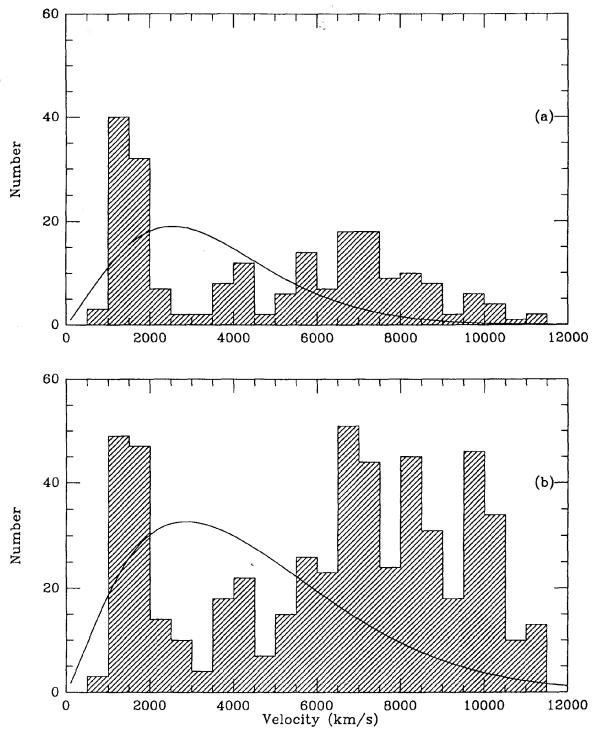

FIG. 4. (a) Histogram of Hubble velocities V_H of the 225 galaxies in the restricted redshift sample. The smooth curve represents the expected distribution for a homogenous population. (b) Same as 4(a), but for the CGCG redshift sample.

density enhancements which were seen in Fig. 4 are present, and the distribution fills nearly the whole redshift range. In addition, this section includes most of the galaxies in the restricted redshift sample near 4000–5000 km s^{-1}, and their number is well above the expectation. Displayed in Fig. 6(b), the second, larger sector, covering the right ascension range $14^h07^m < \text{R.A.} < 14^h50^m$, is even more underpopulated at that distance than was suggested by Fig. 4. This zone contains low velocity objects at $V_H \simeq 2000$ km s^{-1} and ones at $V_H \simeq 7000$ km s^{-1}. The low velocity enhancement includes the Virgo III galaxy cloud. The same absence of galaxies at 3000–5000 km s^{-1} is seen in the third narrow sector, covering the region $14^h50^m \leqslant \text{R.A.} < 15^h12^m$ around the NGC 5846 group [Fig. 6(c)]. The last subregion, the area between $15^h12^m \leqslant \text{R.A.} < 16^h$, is shown in Fig. 6(d) to be lightly populated, especially between 3000–8000 km s^{-1}, a gap which remains unfilled if all 133 galaxies of known redshift in the overall redshift sample are used (single hatching). A strong concentration of galaxies appears at $V_H \simeq 10\,000$ km s^{-1} which can be identified as the southern portion of the Hercules supercluster. The region around R.A. = 15^h10^m to 15^h20^m, Dec. = +7° to +9° contains three Abell clusters: A2040 ($z = 0.0456$), A2052 ($z = 0.0348$) and A2063 ($z = 0.0337$). The latter two contribute an excess of galaxies at the faint magnitude end of the CGCG. Note that this structure is only suggested in the restricted redshift sample itself. Clearly, a deeper redshift survey will be necessary in order to study adequately this volume.

Figure 7 shows cone diagrams with right ascension as the angular coordinate of (a) the restricted redshift sample and (b) the entire redshift sample. In this and the next figure, different symbols are used to indicate group members in the three redshift regimes, as in Fig. 5. Because the percolation algorithm is run only on the restricted redshift sample, this representation is used only in the display of that sample. While its incompleteness towards higher velocities should be kept in mind, Fig. 7(b) clearly shows a progression in the velocity of the density concentration around Zw 1400 + 0949 at $V_H \simeq 7000$ km s^{-1} towards higher velocity until R.A. $\simeq 15^h$ where the 10 000 km s^{-1} Hercules feature

TABLE 2. Groups with density contrast of 20 or greater.

Name	<R.A.>	<Dec.>	#	<V_H>	σ	r_H	M/L	note
Filament	14.15	8.42	59	6832	1413	2.3	651	(a)
IC 989	14.21	4.32	5	6867	1116:	0.39	1161:	(b)
CfA 139	14.31	3.60	7	1797	143	0.10	27	
Vir III	14.60	2.48	18	1975	206	0.63	112	(c)
N 5718	14.63	3.57	3	8584	425	0.13	39	
IC4493	14.72	11.82	5	9082	328	0.39	31	
N 5792	14.88	−1.47	3	2126	48	0.53	50	
CfA 148	14.85	3.75	5	1816	70	0.07	8	
IC1078/9	14.90	9.53	3	8821	173	0.13	6	
N 5846	15.06	1.93	14	1996	381	0.20	163	(d)
N 5940	15.34	8.02	6	10589	594	2.31	194	(e)

Notes to TABLE 2

(a) This extended feature includes the Zw1400+0949 (NGC 5416) cluster and the GH groups CfA 130 and 136.
(b) This group is probably not a physical association, but consists of several objects projected along the same line of sight.
(c) This group is also called dV29 and CfA 145.
(d) This group is also called dV50 and CfA 150.
(e) This group contains the brightest galaxies in the two rich clusters A2052 and A2063.

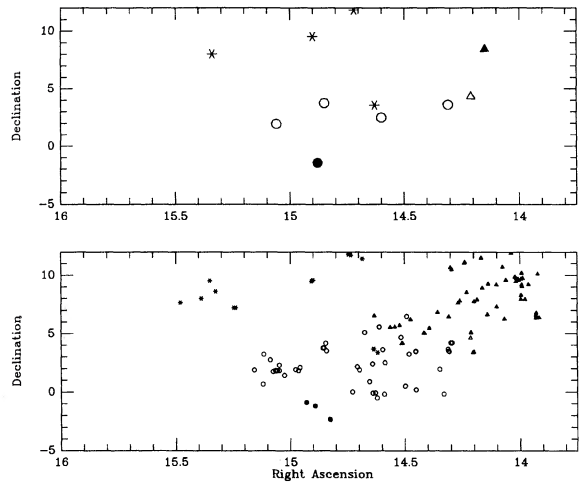

FIG. 5. Similar to Fig. 1, but showing, in the lower panel, the sky distribution of members of the main structural features identified in Table 2 and, in the upper panel, the mean positions of the groups themselves. Circles denote objects with $V_H \leqslant 3000$ km s^{-1}; triangles, those with $V_H \simeq 7000$ km s^{-1}; and asterisks, those with $V_H > 8000$ km s^{-1}. The use of both filled and unfilled symbols is only to allow identification of objects in adjacent structures at the same redshift.

begins. Correspondingly, few galaxies lie between the high and low velocity concentrations east of R.A. $\simeq 14^h$. In Fig. 8, similar cone diagrams are presented for the two samples, but with declination as the angular coordinate. Examination of both Figs. 1(a) and 1(b) and 8(a) shows that the number of bright CGCG ($m \leqslant 14.9$) galaxies falls off towards the south, especially towards the east and that no structure can be traced in that direction. In fact, most of the high velocity galaxies are found north of Dec. $\sim +9°$. Freudling (1990) has already noted that the southern edge of the supercluster appears to be reached south of Dec. $\sim +10°$.

The structure elongated in the radial direction seen at R.A. $\simeq 14^h$ in Fig. 7 is identified as the Zw 1400 + 0949 cluster. As noted by Chincarini *et al.* (1979), at least three clumps exist, strung out in velocity. This distribution does not at all resemble a "finger of God" centered on NGC 5416, but appears more like the discrete clumps found in the Cancer "cluster" (Bothun *et al.* 1983). Inclusion of galaxies fainter than our completion limit only strengthens this impression.

Upon inspection of Figs. 7 and 8, the clump at 7000 km s^{-1} in Fig. 7 now becomes just the northwest end of a long, clumpy, low-contrast linear structure which extends southeast towards roughly (14^h40^m, $+3°$), increasing in mean velocity by perhaps 1000 km s^{-1} as it does so (with substantial spread at any one position). We shall refer to this feature as the "filament," a term used for lack of a better one, but not meant to identify a strictly highly prolate structure. At this (subjective) point in the analysis, we thought that perhaps the filament was in fact a "Y", with another branch moving northeastward from the clump at Dec. = 0° in Fig. 8. This identification later turned out to be more imagination than insight (see Sec. *3.2*). Examination of the redshift distribution of the portion of the sky westward of our survey region suggests, but does not confirm in any believable way that the structure continues westward of this survey boundary of 13^h45^m toward the Coma/A1367 supercluster.

Similar cone diagrams for the low-velocity galaxies only are presented in Figs. 9 and 10 to allow examination of the details of the structure within the Local Supercluster. Here, different symbols are used in the displays of the restricted redshift sample to identify galaxies in separate groups found by the percolation analysis (Table 2). The major impression from these diagrams is that the galaxies mostly fall between 1000 and 2000 km s^{-1}, and lie southward of about Dec. = +5°. In general, the condensations in this redshift

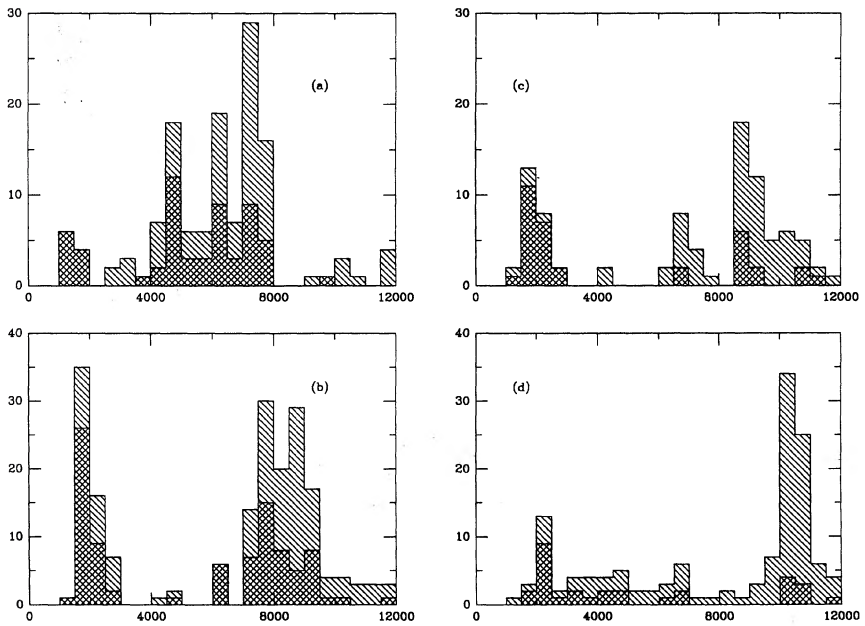

FIG. 6. Histograms of the velocity distributions in four specific zones of right ascension: (a) $13^h52^m \leqslant$ R.A. $< 14^h07^m$; (b) $14^h07^m \leqslant$ R.A. $< 14^h50^m$; (c) $14^h50^m \leqslant$ R.A. $< 15^h12^m$; (d) $15^h12^m \leqslant$ R.A. $< 16^h00^m$. Single hatching indicates the distribution of galaxies in the CGCG redshift sample. Cross hatched areas show the distribution of galaxies in the restricted redshift sample.

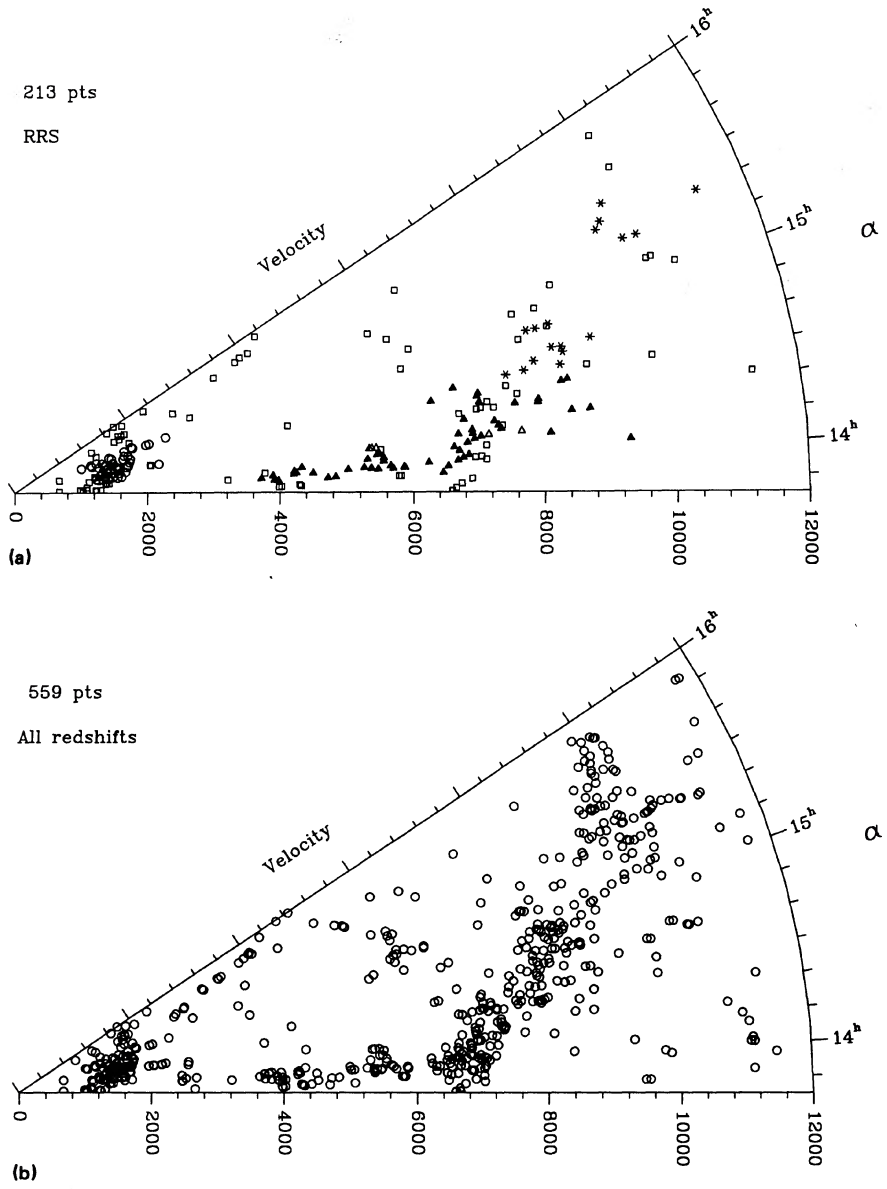

FIG. 7. Cone diagrams with right ascension as the angular coordinate for (a) the restricted redshift sample and (b) the entire redshift sample. In the display of the restricted redshift sample, galaxies that are members of the main structural features identified in Table 2 are marked with different symbols as in Fig. 5, and open squares identify objects not found to be members of any group.

range are not well delineated, justifying Tully's (1982) use of the term "cloud" for the entire region—and so Figs. 8 and 9 are more difficult to analyze than are Figs. 7 and 8. For this reason, we include Figs. 11 and 12. Figure 11 shows a cone diagram with declination as the angular coordinate of the narrow region of right ascension containing the NGC 5846 group, also displayed in Fig. 6(c), $14^h < \text{R.A.} < 15^h12^m$. The NGC 5846 group resembles a compact group with a characteristic "finger of God" velocity distribution, much moreso than does the Zw 1400 + 0949 cluster. Figure 12 shows the velocity histograms constructed for members of the individual low velocity aggregates: the NGC 5846 and Vir III groups and those designated CfA 139 and CfA 148. We do not include the fifth group around NGC 5792 because it contains only three members. The NGC 5846 group stands out because of its larger velocity dispersion. Examination of these diagrams collectively leads us to conclude that the low velocity objects describe a distribution that is indeed prolate, flattened in velocity space and in declination, as was noted by Tully (1982). Note that Tully refers to this entire structure as the Virgo III cloud, whereas dV reserves this term for the concentration near 14.6 hr. We use the term "nearby cloud" for Tully's cloud. The nearby cloud is indeed above and far from parallel to the supergalactic plane, as Tully shows, but his assertion that it points toward the Virgo cluster less conclusive. Figure 10 gives a hint of an increase in mean velocity as one moves from west to east. However, Fig. 12 shows that this effect is smaller than the spread in velocities in any one part of the nearby cloud, and therefore is questionable. Furthermore, it is by no means clear that the necessary NW–SE tilt in the plane of the sky is present. We defer further discussion of this point to Sec. *3.2.*

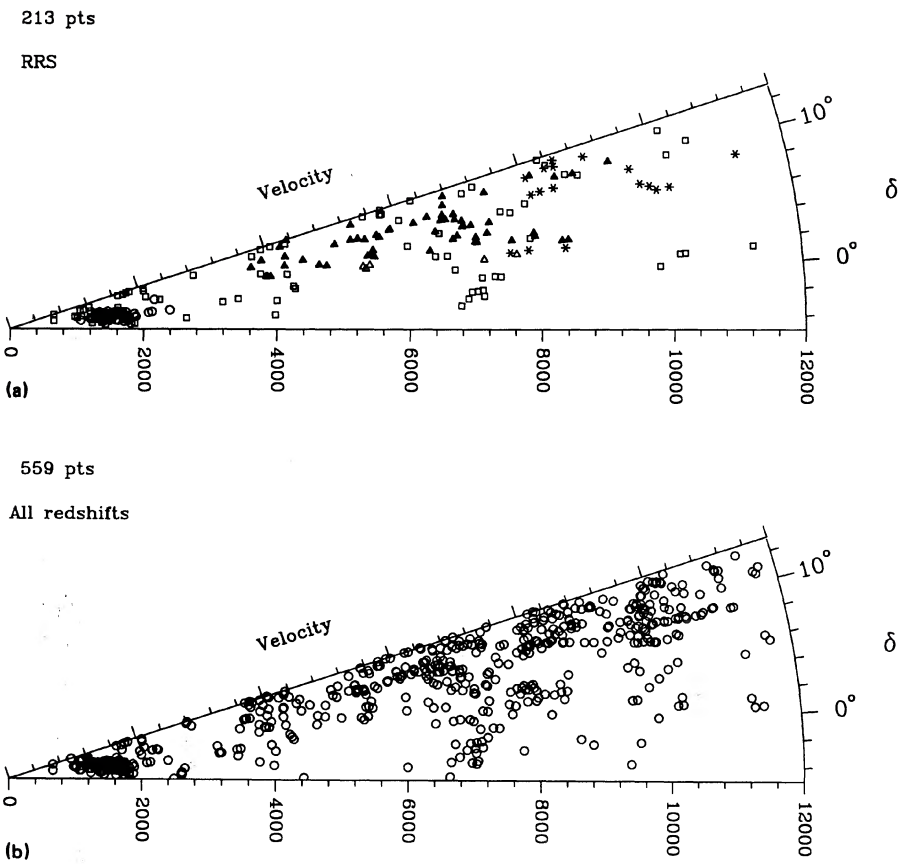

FIG. 8. Cone diagrams, with declination as the angular coordinate, for the restricted redshift sample (a) and the entire redshift sample (b). In the display of the restricted redshift sample, galaxies that are members of the main structural features identified in Table 2 are marked with different symbols as in Fig. 5, and open squares identify objects not found to be members of any group.

In summary, we have visually examined the distribution of bright galaxies in the study region. This examination was performed prior to the objective analysis described in Sec. *3.2,* so as to avoid biasing our findings with knowledge of the numerical results. Because of this, we will claim that structures delineated using both methods are highly likely to be real, and not simply artifacts of human pattern recognition or of unphysical numerical algorithms. Structure exists at two distinct redshift regimes, with a large underdense region between. Furthermore, the CGCG cluster Zw 1400 + 0949 appears not to be a cluster at all, but merely a collection of clumps between $cz = 4000$ and 7500 km s^{-1}, connected at the high-redshift end to an extended (> 10 Mpc), tenuous filament which extends southeastward nearly for some 15°. This filament perhaps is joined from the south by another, even lower contrast structure. At a much closer distance, the prolate cloud described by Tully (1982) is evident, although at this point we can neither confirm nor deny his claim that it points toward the Virgo cluster, particularly since its southerly extent is difficult to determine visually. The data are consistent with the nearby cloud's eastern terminus, the NGC 5846 group, being a gravitationally bound entity; otherwise, substructure is difficult to delineate by eye.

3.2 Automated Cluster Analysis

In order to perform a numerical search for clustering, we must define both a metric and a clustering criterion. The simplest three-dimensional metric uses cz/H_0 as the radial coordinate, but this can lead to clusters which are improperly truncated or subdivided along the line of sight, due to apparent elongation caused by peculiar radial velocities (the "finger of God" effect). Materne (1978) and Tully (1980) have used a simple scaled metric, in which the radial coordinate is scaled relative to the two angular ones by an arbitrary constant. However, as Materne points out, there is no objective way to vary this parameter with redshift so as to study simultaneously structure at different redshifts. For instance, application of Materne's algorithm to our data, using a single scaling parameter for all redshifts, resulted in far-flung pairs of distant galaxies clustering before obvious nearby groups such as that about NGC 5846. Huchra & Geller (1982, hereafter referred to as HG) and GH employ percolation, in which separation is a binary variable: either greater than or less than some cutoff value. Although, for any pair of objects, the mean redshift is used to convert angular separation to linear projected separation, the radial coordinate is nonetheless effectively scaled through the choice of independent cutoffs in redshift separation and in projected separation. How do we decide which groups of galaxies should be considered clusters, and which clusters are more tightly clustered than others? We discuss three basic methods here. Materne (1978) describes hierarchical clustering methods which operate in conjunction with the simple scaled metric mentioned above, and which treat all galaxies and groups of galaxies (hereafter referred to as "clusters") as being equal. Two clusters are joined into a single cluster if they are closer to each other than are any other two clusters, or if the merger

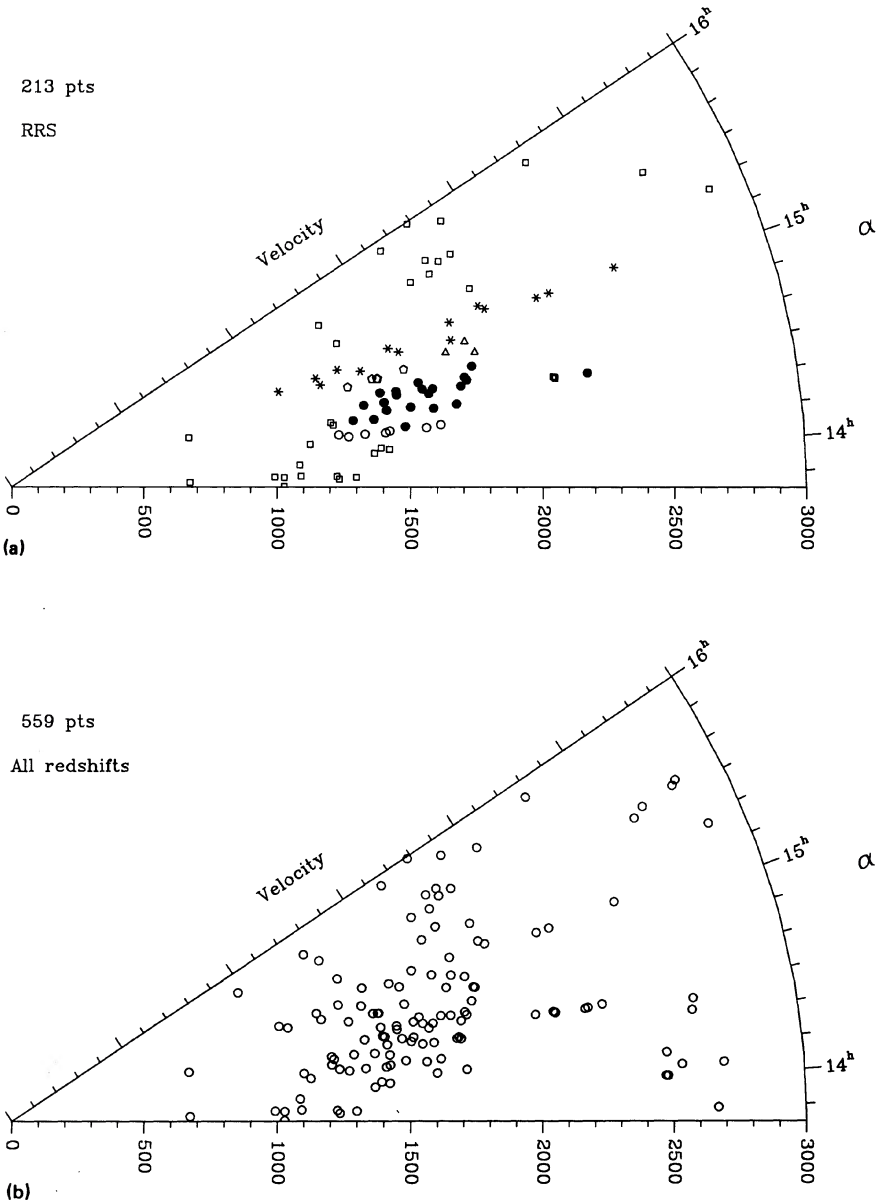

FIG. 9. Cone diagrams, with right ascension as the angular coordinate illustrating the low-velocity structure with $V_H < 3000$ km s^{-1}, for the restricted redshift sample (a) and the entire redshift sample (b). In the display of the restricted redshift sample, galaxies that are members of the main structural features identified in Table 2 are marked with different symbols. Unlike the representation in Fig. 5, here members of the five low velocity groups are identified separately. Open squares identify objects not found to be members of any group.

results in the smallest increase in positional dispersion of all possible mergers (the "Ward criterion"). Note that in the former case, the relevant distance can be that between the nearest two member galaxies ("single linkage"), between the farthest two member galaxies ("complete linkage"), or between the cluster centroids ("centroid clustering"). As this process is carried out, the sample is transformed from N one-galaxy clusters to one N-galaxy cluster, producing a hierarchy of cluster lists along the way.

Tully (1980) has criticized this class of clustering criteria as being unphysical, since it treats large galaxy groups on an equal basis with single galaxies. He proposes the use of centroid clustering, with inverse gravitational force replacing three-dimensional separation as the quantity to be minimized in determining which two clusters will merge at any given step in the hierarchy. A large cluster which has formed in previous steps now is much more likely to "accumulate" a test particle than is a single galaxy at the same distance. However, one result of this, as Tully notes, is that subclustering is strongly suppressed. Indeed, in applying this algorithm to our data, we found that one or two tightly bound clusters formed early on, and proceeded to accumulate galaxies one at a time until the supply was exhausted. This too can be considered an unphysical result, an artifact of the hierarchical algorithm. At any step, only the two most strongly attracted clusters are permitted to merge, whereas in reality, test particles react to strong, moderate, and weak forces simultaneously, leading to the subclustering generally seen in N-body simulations (Fitchett 1990) and even in rich galaxy clusters (West & Bothun 1990). Other problems with this clustering criterion are the necessary use of mass-to-light ratios and of the simple scaled metric, and the assumption that even elongated clusters act as point masses located at the cluster centroids. For these reasons we have used neither Tully's nor Materne's methods in our final analysis.

Instead, we have adopted the percolation technique of HG

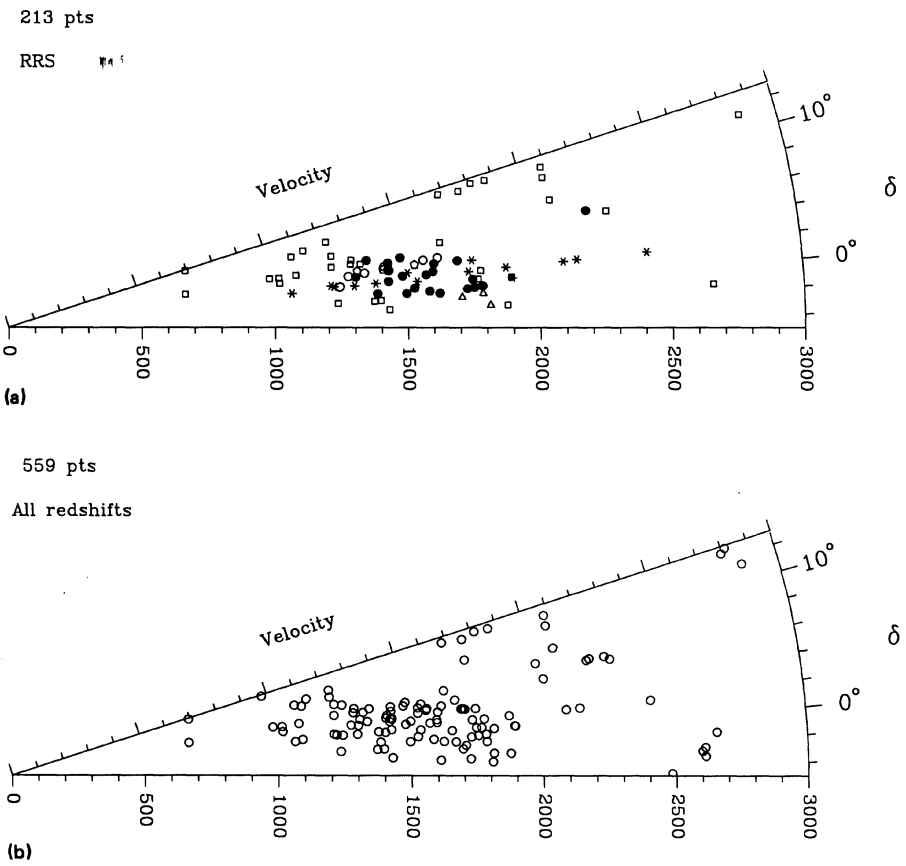

FIG. 10. Cone diagrams, with declination as the angular coordinate illustrating the low-velocity structure with $V_H < 3000$ km s^{-1}, for the restricted redshift sample (a) and the entire redshift sample (b). In the display of the restricted redshift sample, galaxies that are members of the main structural features identified in Table 2 are marked with different symbols as in Fig. 9, and open squares identify objects not found to be members of any group.

and GH. This is similar to single linkage clustering in that nearest-neighbor distances are effectively used, and in that all galaxies are equal. However, because the metric depends on two parameters which can be varied independently, a unique hierarchy does not exist. For given values of these two maximum separations, though, the resulting list of clusters *is* unique and reproducible. Essentially, by ignoring gravity, reducing separations to binary variables, and letting the relationship between velocity separation and projected separation be a free parameter, we are admitting that we do not yet understand well the nature or causes of structure in the universe.

Our methods are identical to those described at length by HG. For each ungrouped galaxy, we inspect all other ungrouped galaxies, checking whether both redshift separation and projected linear separation are below specified cutoff values (which both are allowed to increase with increasing mean redshift in order to compensate for Malmquist bias). If such is the case, the second galaxy is grouped with the first; later, companions of this second galaxy are sought and added to the group, etc. We used the magnitude completeness limit of 14.9, and the corresponding absolute magnitude function parameters fit by us in Sec. *2.2,* in correcting for Malmquist bias.

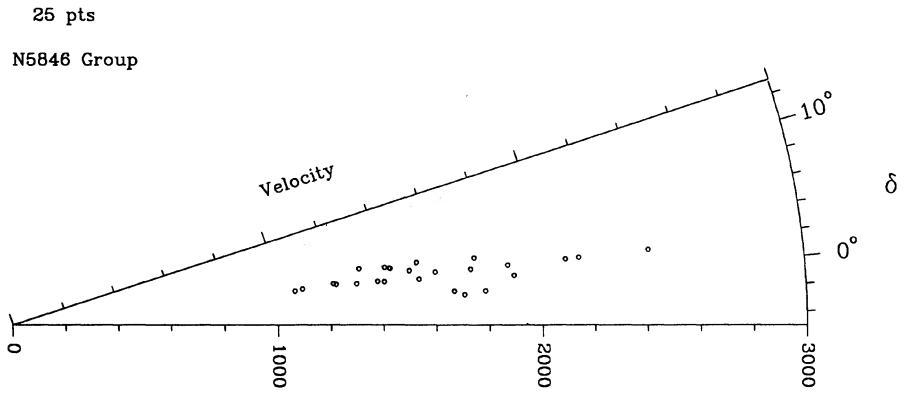

FIG. 11. Cone diagram with declination as the angular coordinate in the narrow zone of right ascension surrounding the NGC 5846 group $14^h50^m \leqslant$ R.A. $< 15^h12^m$. All galaxies with measured redshifts are included.

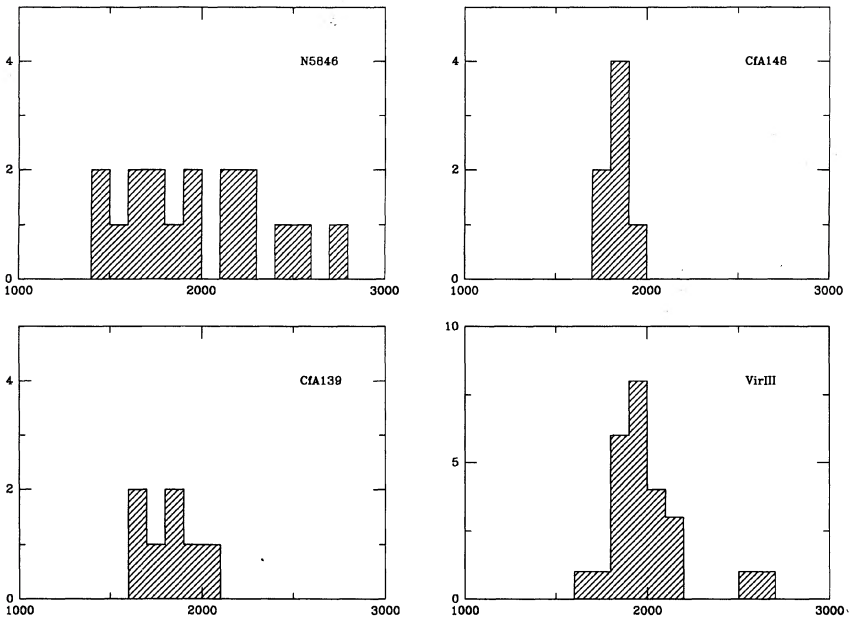

FIG. 12. Redshift histograms for galaxies in the four more populous low velocity groups found in the revised redshift sample.

As discussed in Sec. *2.2,* a maximum redshift cutoff must be imposed on the sample in order to use properly this method. In checking whether a nearby galaxy should be grouped with a very distant one, the degree of Malmquist bias is estimated using the mean Hubble distance, which, in this case, will be about half of a large number: still fairly large. The resulting correction can be so large, and the separation cutoffs so enormous, that the two galaxies may well be grouped together. The end result is a single "supergroup", consisting of nearby galaxies from all over the sky and, say, one galaxy at $cz = 30\,000$ km s^{-1}. Perhaps the use of harmonic distances, rather than mean distances, in compensating for Malmquist bias would alleviate this problem, but we (and evidently HG) found a redshift cutoff to be more convenient. The number density contrast between delineated features and the mean density of our sample is set by the projected separation cutoff and by the absolute magnitude function fit in Sec. *2.2;* by Eq. (4) of HG,

$$\text{contrast} \sim 20(D_0/0.5\ \text{Mpc})^{-3},$$

where D_0 is the cutoff for two galaxies at a fiducial mean redshift $V_F = 1000$ km s^{-1}. At the same fiducial redshift, we also required grouped pairs to differ in radial velocity by less than 600 km s^{-1}. This value of the radial velocity difference $\Delta V = |V_1 - V_2|$ turns out to be large enough that the velocity dispersions within the resulting groups are substantially smaller than the Malmquist-corrected velocity separation cutoff V_L at the mean group redshift, which means that we are properly allowing for artificial elongation in this dimension. We also used values of $\Delta V = 400$ km s^{-1} and 200 km s^{-1}, to see if lowering ΔV at fixed D_0 would cause any large, diffuse groups to break up into two tightly bound subgroups along the line of sight. In fact this seldom occurred: Once V_L approached the group velocity dispersion, one member at a time would be eliminated from the group. For this reason we will present results obtained with $\Delta V = 600$ km s^{-1} unless otherwise specified. We note that this is the value used by GH for their analysis of a sample complete to $m = +14.5$, nearly as deep as ours.

We have used percolation techniques to produce a list of galaxy groups with number density a factor of 20 (or more) above the mean density for our sample. This list is completely analagous to the catalogs of HG and GH. Because of difficulties with boundary effects, we present results only for groups centered east of R.A. = 14^h, although we include objects within the western extension of the survey region. As already noted, the paucity of objects towards the east decreases the chances of finding structures there anyway. In Table 2, we present our results for contrast = 20, the value for which the group lists of HG and GH are defined. Eleven groups are thus selected from our sample to meet the contrast criteria and to contain three or more members and positive corrected velocity dispersions. Eight of these groups contain five or more members in the complete sample and as such are free of incompleteness problems. For each group, Table 2 lists the group name, the mean position, ⟨R.A.⟩ and ⟨Dec.⟩; the number of members #; the mean Hubble velocity $\langle V_H \rangle$; the radial velocity dispersion, σ, corrected by subtracting in quadrature the rms observational velocity error; the mean harmonic radius, r_H; and the derived virial mass-to-light ratio $\mathcal{M}/L$. The harmonic mean radius is defined by

$$r_H = \frac{8}{\pi}\frac{\langle V \rangle}{H}\sin\left(\frac{1}{n(n-1)}\sum\frac{1}{\theta_{ij}}\right)^{-1}. \quad (1)$$

Equation (1) corrects an interchange of leading coefficients (i.e., projection correction factors) between HG's Eqs. (13) and (14) for mean harmonic radius and mean pairwise separation, and a typographical error in their Eq. (13). For each group, a virial mass has been calculated using the virial mass estimator given by Heisler *et al.* (1985). From this, the mass-to-light ratio has been derived in a straightforward manner calculating luminosities from observed CGCG magnitudes following the prescription described in Haynes & Giovanelli (1984). This ratio is meant only to be used for

comparative purposes and is not to be taken too literally. Its most significant use is in tracing the reality of groups where the number of members is small: large jumps in increasing $\mathcal{M}/L$ occur when nonmembers are included by the percolation algorithm in group assignments (Puche & Carignan 1988).

Note the absence of nearby structure eastward of the NGC 5846 group. The number of cataloged objects falls off rapidly as the supergalactic latitude grows and the galactic latitude falls. On the other hand, the lack of redshift coverage towards the south does affect the analysis. The group around NGC 5792 lies on the very southern edge of the survey and may be incompletely identified. Because it has only three members in the current restricted sample, we will not discuss its structure further. If we extend the analysis including objects with Dec. $< -2.0°$, despite the lack of completeness we find several additional groups emerge from the percolation. One of those, around the galaxies NGC 5506/7, has five members. Both of these groups are also members of the "nearby cloud", having $\langle V_H \rangle \simeq 2200$ km s^{-1}. The full extent of the large scale structure is limited by the survey coverage, but at the same time, analysis of the groups defined by the contrast limit of 20 can proceed.

Application of the percolation algorithm confirms the general subjective impressions of the large scale structure in the region corresponding to a contrast of about 10. At this level, the four clumps—CfA 139, Virgo III, CfA 148 and NGC 5846—comprise the "nearby cloud" identified in Sec. *3.1* and by Tully (1982). Albeit with much spread in the velocity and declination dimensions, three of the groups—CfA 139, Virgo III and NGC 5846—exhibit an increase in mean velocity and a decrease in mean declination eastward as apparent also in Figs. 8 and 9. This trend can be understood if the cloud points towards the Virgo cluster, as proposed by Tully. The ambiguity of the trend in declination, mentioned in Sec. *3.2,* is alleviated in this analysis by the fact that the percolation algorithm has excluded the galaxies in the southwestern corner of the region of study from the cloud. At the same time, CfA 148, a very compact group, is too far north and has too low a velocity. Perhaps this clump formed from leftover gas that was never associated with the nearby cloud. Alternatively, in an intermediate stage of the collapse and tidal distortion of a protocloud which will eventually produce 50 or so galaxies, it is not unlikely that a small subclump, from which will form only five galaxies, could break off. In either case, we conclude that Tully (1982) is correct is his description of the nearby cloud, but encourage deeper optical and H I redshift surveys through which one can investigate the low mass members.

As the contrast level grows to exceed 20, some of the identified groups quickly break apart. At contrast = 40, Virgo III is reduced to 15 members with a fairly low $\mathcal{M}/L$ (44). It does not look like a bound structure, but appears instead much like a horseshoe centered at R.A. = 14^h36^m, Dec = $+1°$ so that virial estimates are probably meaningless. At contrast = 100, this horseshoe breaks into two clumps of five members, plus several smaller entities. CfA 139 loses a member (UGC 9215) at this same contrast, and becomes an extremely tight ($\mathcal{M}/L = 12$) six-member group that remains clustered until contrast = 3000. CfA 148 remains intact until contrast = 1000, when it loses one member NGC 5770. The group around NGC 5846 contains 12 members at contrast = 100. At contrast = 300, it splits into two subclumps of 9 and 3 galaxies, respectively. The smaller clump around NGC 5813 remains intact to contrast = 30 000. The main NGC 5846 group itself is composed of 7 members at contrast = 1000 and still 5 at contrast = 30 000, and shows no evidence for substantial reduction in $\mathcal{M}/L$ with increasing contrast.

At larger distances, because of the rather bright magnitude limit imposed on the resticted redshift sample, we see only the highest density features but their presence in this region is obvious. At contrast 10, almost the entire sample percolates into either the nearby cloud discussed above or a high velocity feature connecting from the Zw 1400 + 0949 filament to the Hercules supercluster. The three groups with highest mean Hubble velocity are located in the northern portion of the survey region and are probably associated with local density enhancements within the southern extension of the Hercules supercluster. In fact, the group whose brightest member is NGC 5940 actually consists of the brightest objects in two Abell clusters A2052 ($cz = 10\,400$) and A2063 ($cz = 10\,100$). Because only the brightest galaxies in these structures are included in the redstricted redshift sample (evidenced also in the comparison of different panels in Figs. 6, 7 and 8), the group properties derived by the percolation algorithm have little true meaning and these aggregates will not be discussed in any detail.

Despite its much greater distance, the filament extending from Zw 1400 + 0949 is impressively durable. Group membership and $\mathcal{M}/L$ drop from 59 and 651, respectively, at contrast = 20, down to 12 and 105 at contrast = 300. The large change in $\mathcal{M}/L$ is indicative that the feature is not a single, bound structure. At such a high contrast, the original filament is reduced to the primary members of the Zw 1400 + 0949 group. The structure represents a strong density enhancement, even though it has a high velocity dispersion and spans the three subclumps identified visually in Sec. *3.1.* Although the use of $\Delta V = 200$ km s^{-1}, for any value of contrast, breaks off the low velocity clump, the group velocity dispersion is often nearly equal to ΔV, an unacceptable situation, and the discrepancy between subjective and objective clustering is still not fully resolved. We propose that the structure in Zw 1400 + 0949 should be considered neither discrete clumps nor a "finger of God" but rather a single, truly prolate cloud, parallel to the line of sight, within which lie several condensations.

Note that if $\Delta V = 200$ km s^{-1}, the filament breaks into tight clumps at contrast = 20, but such a value of ΔV is too low for a density contrast of only 20 and will artificially disallow extended structure that is not perpendicular to the line of sight. At contrast = 10, the Zw 1400 + 0949 cluster merges with the filament to form a single structure, strung out over 4000 km s^{-1} in velocity space. Since this cloud appears to point in the direction of the Coma cluster, we performed the group search on a sample of galaxies between $13^h <$ R.A. $< 15^h$, and $0° <$ Dec. $< +40°$ in order to look for a connection. The same magnitude limit was imposed. No extension of the filament west of the region of study was seen, whereas the extension of the Coma-A1367 supercluster northeastward from Coma shows up clearly. Therefore, our western boundary does not artificially terminate the filament at a contrast level of 20. The reality of the termination is also seen in the luminosity contour diagram presented as Fig. 3 of HG. As a further check, we performed a third search for structure of a large section of the Pisces–Perseus supercluster whose main ridge is a striking linear feature in the resulting group list (Wegner *et al.* 1990). A comparison

between the filament/Zw 1400 + 0949 structure and Pisces–Perseus should be performed at contrast = 40 for the latter to compensate for its smaller distance. Using that level, the main ridge of Pisces–Perseus divides into two filamentary groups. The structure seen in the region discussed here at $\simeq$7000 km s^{-1} is significantly more tenuous than that seen either in the Coma-A1367 or Pisces–Perseus superclusters. In light of this lowered contrast, the fact that the purported connection with a southern branch (see Sec. *3.1*) does not appear in our objective analysis, even at a contrast of 10, indicates that this branch cannot be considered real, at least given the currently available data. The confirmation of the elongated structure in the direction of Zw 1400 + 0949 and how and why it connects at right angles to the long, tenuous filament awaits the extension of the redshift survey to fainter magnitudes.

The study of the Zw 1400 + 0949 cluster clearly brings out the fact that percolation and other automated clustering algorithms are useful mechanical tools, but require a measure of subjective input nonetheless. Our visual impression of that region had to be utilized in understanding the structure; the clumpiness apparent in cone diagrams refused to meet the clustering criteria of the numerical analysis. In addition, subjectivity enters in setting "approximate" density contrasts and radial velocity separation cutoffs, and in deciding how to interpret virial mass-to-light ratios. Small number statistics force the investigator not to accept numerical results at face value. For example, while magnitude incompleteness can be addressed on a statistical basis, a single missing galaxy may cause a group to appear as two smaller ones. It is difficult to describe quantitatively the morphology of loose aggregates containing few galaxies. Also, it is difficult to determine whether or not raising the required contrast level "disintegrates" a given aggregate, since most are small even at contrast = 200. For these reasons, we have kept this discussion largely descriptive, so as not to rely too heavily on the precise group membership and numerical properties.

4. COMPARISON OF GROUP PROPERTIES

In the previous section, we have examined the three-dimensional structure within the region around NGC 5846 and have identified groups and inspected them for regularity. Eight of those groups contain five or more members north of the redshift incompleteness limit of Dec. = $-2°$ and can be considered as dynamical units. The eight identified groups occupy two distinct redshift regimes and are all quite different. At higher velocities, within the limits imposed by sampling only the bright end of the luminosity function, we cannot say too much about specific group properties. The Zw 1400 + 0949 cluster itself is moderately dense but not very regular and the $cz \simeq 7000$ km s^{-1} "filament" appears to be a loose, irregular structure. Even among the lower velocity aggregates, all likely members of the same galaxy "cloud", the degree of concentration and symmetry properties vary among the four separately identified clumps. Only the NGC 5846 group itself is both regular and condensed. While similarly compact, CfA 139 and CfA148 cannot be tested for symmetry because of their small memberships. The grouped labelled Virgo III in comparison is significantly less condensed and less regular.

Because their much greater distance renders the search for companions difficult in our catalog and gives rise to greater uncertainties in measured parameters, the properties of galaxies in the filament will not be discussed further. Several authors have already shown (Schommer *et al.* 1981; Chincarini *et al.* 1981; Giovanelli and Haynes 1985) that spiral galaxies in Zw 1400 + 0949 are relatively H I normal when compared with objects of similar morphology and size in the field. While the concentration around Zw 1400 + 0949 and the extension in the filament are clearly well identified by the percolation algorithm, the large velocity spread and projected maximum dimension classify them by somewhat different criteria. Their distinctiveness is partly enhanced because they lie at precisely the distance where the peak of the redshift distribution corresponding to a catalog with a limit of -14.9 and the characteristics of the luminosity function combine to enhance the apparent structure in the current sample.

The most striking density enhancement in the study region, the NGC 5846 group, is one of the few groups in the list of dV which is composed mostly of early type galaxies. By analogy with the properties of rich clusters (Melnick & Sargent 1978; Dressler 1980), we would expect the group to be centrally condensed and to appear symmetric in angle and in radial velocity. The denser regions of the group should contain earlier galaxies than do the outskirts. If environmental interactions are sufficiently dramatic, spirals which are found in the core might also be H I deficient (Haynes *et al.* 1984). The mass-to-light ratio should be low, although the possibility of dark matter complicates the interpretation of measured values.

The four groups at low velocity are all associated with the "nearby cloud" and as such, can be compared with minimum concern for distance bias effects. In measuring group properties, we first defined rough group borders in three dimensions, using the percolation results of Sec. *3.2* for contrast = 20. For each group, we construct two samples: one which contains all galaxies in the magnitude-limited redshift sample included in the group by application of the group finding algorithm described above; and one which contains all galaxies in the redshift catalog which are fainter that the magnitude limit, but lie within the same volume. Of the latter, we have also examined the H I sample mentioned previously. Our goal is to investigate the mean properties of galaxies in these local aggregates and to compare these groups with other concentrations in the Local Supercluster. The mean properties are derived for aggregates defined by the percolation algorithm at contrast = 20 and hence are useful only for comparison with aggregates defined in the same manner. Comparisons between individual groups have been performed quantitatively by comparing distribution functions (Kolmogorov–Smirnov test). Because of small number statistics and uncertainties in the inferences about physical groupings that are identified by the automated percolation procedure, these results can indicate trends only.

Table 3 presents in summary form the results of our comparison of the mean morphology and H I content of group members. Because of the small populations of these groups, the comparison is performed only between these two general group properties: the mean morphology $\langle T \rangle$, coded according to the scheme of deVaucouleurs *et al.* (1976) and the mean H I deficiency $\langle$DEF$\rangle$, defined as the difference between the observed H I mass and that predicted for a galaxy of similar morphology and linear diameter as discussed by Haynes *et al.* (1984). The classification comes from the Revised Shapely Ames Catalog (Sandage & Tammann 1988) where available or else has been performed by us using

TABLE 3. Comparison of nearby groups at contrast 20.

Name	N_T	<T>	s.d.	N_{HI}	<DEF>	s.d.
CfA 139	7	2.0	3.8	4	+0.25	0.4
Vir III	18	3.2	3.2	18	−0.01	0.2
CfA 148	5	3.6	3.4	5	−0.05	0.2
N 5846	14	−0.1	4.4	6	+0.32	0.2
M 96	14	2.0	4.3	7	+0.14	0.4
N 3607	15	2.0	4.6	8	+0.10	0.4
N 3628	11	3.5	2.5	7	+0.16	0.2
U Ma	117	2.1	4.2	138	+0.30	0.5
Virgo	224	1.8	4.4	45	+0.36	0.4

plate reproductions of the PSS plates. In computing $\langle T \rangle$, we have included all nonpeculiar galaxies in the restricted redshift sample to measure the morphological properties. No correction has been applied for the discreteness of T. The number of galaxies contributing to $\langle T \rangle$, N_T is also listed. Note that the the determination of the H I deficiency parameter is only valid for types Sab through Irr and hence the H I comparison has been restricted to galaxies of those classifications, but not merely to the bright galaxy sample. The number $N_{\rm H\,I}$ of galaxies used in the determination of the mean deficiency is also listed in Table 3. The calculation of a mean deficiency is complicated by the likely contamination by H I normal objects, seen in projection but actually not located in a high density region, a case such as that seen in the Virgo core (Haynes & Giovanelli 1986a). Haynes *et al.* (1984) found for their isolated galaxy sample a standard deviation of 0.24 around the mean in $\log(M_{\rm H\,I}/D_I^2)$, so that, with the small numbers of spiral objects included here, the evaluation of mean H I deficiency is crude at best.

For comparative purposes, we have also run the percolation algorithm at contrast = 20 on large regions of the sky surrounding three other well known groups in the Local Supercluster, namely the NGC 3607, NGC 3628, and M96 groups. The redshift catalog we have used for this group identification is also complete at least to a magnitude of 14.9, and we have imposed all of the same limits in terms of magnitude and velocity. These groups are in the well-studied Leo region and span a range of morphological type mix. The NGC 3607 group is similar to the NGC 5846 group in its dominance by early type galaxies. The more prominent and populous Ursa Major and Virgo clusters are also included in the comparison. As suggested by Pierce & Tully (1988), the Ursa Major cluster is assumed to include galaxies within 7.5 degrees of R.A. = 11^h54^m, Dec. = $+49°30^m$ with $700 < V_\odot < 1210$ km s^{-1}. Virgo is restricted to the volume within seven degrees of M87 and $V_\odot < 2800$ km s^{-1}. The radius chosen here roughly corresponds to the contrast = 20 level we have set for the groups identified via percolation. On the other hand, the Virgo core is usually held to a radius of five degrees.

The evaluation of the mean group properties provides an understanding of the NGC 5846 group in terms of conventional theories of the relationship of morphology and local density. The NGC 5846 group has the lowest mean morphological type and the highest mean H I deficiency, as we might have expected, given its high degree of central concentration. In contrast, the Virgo III cloud is composed of late-type, H I normal spirals.

Because these two groups are reasonably large at contrast = 20, we checked whether $\langle T \rangle$ and $\langle$DEF$\rangle$ changed as progressively higher density regions were inspected, making use of the percolated group lists produced in Sec. *3.2*. For Virgo III, $\langle T \rangle$ actually increases slightly as the contrast increases. In the NGC 5846 group, morphological segregation is clearly observed: at contrast = 300, the nine group members have $\langle T \rangle = -1.6$. In Virgo III, the few highly H I deficient (DEF$\geqslant +0.30$) are not preferentially located within dense condensations. In the NGC 5846 group, this test is inconclusive, partly because so few central galaxies are spirals. NGC 5846 itself is a strong x-ray source and in this case, evolution may include the possibility of recent interaction with the hot gas in the halo of NGC 5846 itself (Biermann *et al.* 1989). Bregman *et al.* (1988) place an upper limit of a few times $10^7 \mathcal{M}_\odot$ of H I in NGC 5846.

Despite the much smaller population, the group around NGC 5846 bears some resemblance to the core of the Virgo cluster. As seen in Fig. 12 and quantified in Table 2, the NGC 5846 group has a much larger velocity dispersion than the other nearby loose groups. The five degree core of Virgo shows a mean type $\langle T \rangle$ of 1.8 and a very high degree of H I deficiency $\langle$DEF$\rangle$ of +0.36. It is quite clear that gas stripping of the H I in spirals occurs as they pass close to the center of the Virgo core (e.g., Haynes 1990).

The two smaller groups, CfA 139 and CfA 148 would appear at first to be quite similar objects: small compact (in space and velocity) clumps. In fact, they are quite different. Morphologically, the galaxies in CfA 139 are of earlier type than those in CfA 148. Although the small numbers of galaxies in each group render the difference indicative only, we note that by removing the outlying member of CfA 139, UGC 9215, from the group, we obtain a very tight six-member clump with $\langle T \rangle$ reduced from 2.0 to 1.3, accentuating the difference between it and CfA 148. The strong difference between the two clumps is in their H I properties. CfA 139 is a factor of two deficient in H I, in the mean, relative to spatially isolated galaxies, whereas CfA 148 is H I normal.

The status of the two clumps CfA 139 and CfA 148 is crucial to our interpretation of the entire region. It is difficult to understand their morphological properties if they are transient, unbound density enhancements which have formed within the nearby cloud, as has been proposed as a model for the formation of compact groups by Rose (1979). The fact that CfA 139 contains earlier type galaxies than the nearby Virgo III cloud would seem to be attributed to numerous pair interactions and extremely effective tidal or collisional effects on morphology. Because few interactions will occur if the configuration is transient, we do not consider such an explanation to be plausible. While this problem does not arise in the late-type clump CfA 148, we recall from Sec. *3.2* that this group is somewhat exterior to the nearby cloud, and therefore cannot have formed recently from galaxies orbiting within the cloud. We suggest instead that these clumps are dynamically evolved remnants of loose groups, a possibility that Rose (1979) found difficult to rule out. Presumably CfA 139 started as a small but dense protocloud, whereas CfA 148 was a weaker enhancement which has only recently reached a compact state. This conclusion is based on the relative type indices, and is independent of whether initial conditions or interactions are responsible for galaxian morphology. We tentatively conclude that the groups are ordered in increasing initial density as Virgo III, CfA 148, CfA 139, and NGC 5846. This ordering is the same as that obtained for morphology and for H I content, except that CfA 148 would be placed together with the first three groups

in these two lists. It is therefore impossible to distinguish between congenital and environmental influences on galaxian morphology and gas content, but it is possible to see a threshold effect at work in either scenario. Although CfA 148 is denser than Virgo III, the members of the two groups are equally gas-rich and late-type. Assuming that CfA 148 was initially only marginally overdense relative to Virgo III, this difference might not have been enough to cause any difference in type index (in the "initial conditions" scenario), or else might not have led to significantly more pairwise orbital interactions up to the present (in the "environment" scenario). Note that this analysis is not valid if CfA 148 is, despite our arguments to the contrary, a transient configuration made up of galaxies which formed in an environment just as rarefied as Virgo III.

It might in fact be possible to check for environmental effects on H I content by searching CfA 139 for tidally strewn gas. Since orbital interactions are the only possible environmental effects in this clump, the low type index found here might be accompanied by detectable column densities of unionized hydrogen in the intragroup medium. Similarly, recent morphological modification could be investigated by searching this group for merger candidates. Obviously, it would be useful to study the galaxian morphology and H I content of a large ensemble of small, tight groups, the large number of groups compensating for the small number of galaxies in each group.

5. SUMMARY

We have chosen for study a region of sky in which we could identify large-scale structure within the Local Supercluster, namely the concentration of galaxies around the E/S0 galaxy NGC 5846. Other coherent features are also evident at larger distances. Within this region, which extends from $13^h45^m < \text{R.A.} < 16^h00^m$ and $-05° < \text{Dec.} < +12°$, a redshift sample, complete in magnitude to $m \leqslant +14.9$, has been used to make a visual search for structure utilizing numerous two-dimensional slices through R.A.-Dec.-redshift space, displayed in Fig. 7–11. The results of an automated search, in which a percolation algorithm was applied to the same complete redshift sample, have been compared with those of the subjective impressions.

At a number density enhancement of 20 over the mean background, we identified eight large ($N > 4$) groups which were not affected by incompleteness at very low declinations. Four of these groups–the Virgo III cloud, the NGC 5846 group, and groups 139 and 148 from the list of GH–are nearby, with corrected $cz \simeq 1900$ km s^{-1}. Virgo III is loose and irregular whereas NGC 5846 is dense and symmetric. The other two groups are small, compact clumps. We agree with Tully's (1982) conclusion that these four nearby groups (with the possible exception of CfA 148) form a prolate cloud with an overall density contrast over the mean of about 10, and that this cloud lies out of the supergalactic plane and points toward the Virgo cluster.

Another well-known group, the Zwicky cluster 1400 + 0949, also known as the NGC 5416 group, lies at $\langle cz \rangle \simeq 7000$ km s^{-1}, and has a radial velocity dispersion of over 1000 km s^{-1}. Considering this large dispersion, the clumpy visual appearance of the structure, and its persistence in percolation runs up to large density contrasts, we conclude in agreement with previous authors that the group is not confined to a single core. The galaxies in this region form a prolate cloud, clumped but continuous and moderately dense, whose large velocity dispersion results from fortuitous alignment along the line of sight rather than from orbital dynamics. From the high-velocity end of this cloud stems an extensive "group," a long, nebulous filament which extends nearly 15° as a coherent structure. Although we attempted to allow for Malmquist bias in both the visual and the automated analyses, we note that deeper redshift surveys will be necessary before firm conclusions can be drawn about the detailed structure at $cz \simeq 7000$–8000 km s^{-1}. Although seriously limited by restriction to only the most luminous galaxies, the analysis also identified the southern extension of the Hercules supercluster at $cz \simeq 10\,000$ km s^{-1}.

Having estimated which structures are real and how dense they are, we investigated the morphological and atomic gas properties of the member galaxies of the nearby groups. The loosest group Virgo III is composed of galaxies which are indistinguishable in either respect from spatially isolated galaxies. Of the three dense aggregates, NGC 5846 and (to a lesser extent) CfA 139 are skewed toward early type galaxies and contain spirals which are H I deficient. CfA 148, on the other hand, is composed of galaxies like those in the looser groups. We do not feel that either of the two compact clumps can be considered transient configurations, but suspect instead that they are dynamically evolved versions of what once were loose groups. We hypothesize that CfA 148 formed from a marginally overdense protocloud which has only recently attained a compact form. If this is true, then this clump's H I- normal status can be explained by a lack of past orbital interactions between galaxies, while the late-type index is due to this effect (if galaxy morphology is a product of recent interactions) or directly to a threshold effect (if morphology is a product of initial protocloud density). Even if this explanation can produce a perfect correlation between group properties and member galaxy properties for all six groups, we cannot determine whether this is a result of the latter being dominated by initial conditions or by environmental effects, but we suggest that CfA 139—which contains no hot intragroup gas—be searched for merger candidates and tidally strewn H I, and urge that the galaxian attributes of more compact groups be studied in order to obtain statistically meaningful results.

It is a pleasure to thank the staffs of the Arecibo and National Radio Astronomy Observatories for assistance with the telescope observations. We thank Ann Savage of the UK-Australia Schmidt Telescope Unit for providing us with a film copy of the *J* survey print of the field around NGC 5846. Some of the group analysis was performed with the assistance of Shoko Sakai.

REFERENCES

Biermann, P. L., Kronberg, P. P., and Schmutzler, T. 1989, A&A, 208, 22
Bothun, G. D., Geller, M. J., Beers, T. C., and Huchra, J. P. 1983, ApJ, 268, 47
Bregman, J. N., Roberts, M. S., and Giovanelli, R. 1988, ApJL, 330, L93
Chincarini, G. L., Giovanelli, R., and Haynes, M. P. 1979, AJ, 84, 1500
de Lapparent, V., Geller, M. J., and Huchra, J. P. 1986, ApJL, 302, L1
de Vaucouleurs, G. 1960, ApJ 131, 565
de Vaucouleurs, G., de Vaucouleurs, A., and Corwin, H. G. 1976, Second

Reference Catalogue of Bright Galaxies (University Texas Press, Austin)
de Vaucouleurs, G. 1975, in Galaxies and the Universe, edited by A. Sandage, M. Sandage, and J. Kristian (University Chicago Press, Chicago), p. 557 (dV)
Dressel, L. L., and Condon, J. J. 1976, ApJS, 31, 187
Dressler, A. 1980, ApJ, 236, 351
Faber, S., and Burstein, D. 1988, in Large Scale Motions in the Universe, edited by V. C. Rubin and G. V. Coyne (Princeton University Press, Princeton), p. 116
Fitchett, M. J. 1990, in Clusters of Galaxies, edited by W. R. Oegerle, M. J. Fitchett, and L. Danly (Cambridge University Press, New York), p. 111
Fontanelli, P. 1984, A&A, 138, 85
Freudling, W. 1990, Ph.D. thesis, Cornell University
Freudling, W., Haynes, M. P., and Giovanelli, R. 1988, AJ 96, 1791
Geller, M. J., and Huchra, J. P. 1983, ApJ, 52, 61 (GH)
Giovanelli, R., and Haynes, M. P. 1982, AJ, 87, 1
Giovanelli, R., and Haynes, M. P. 1985, ApJ, 292, 404
Giovanelli, R., Haynes, M. P., and Chincarini, G. L. 1986, ApJ, 300, 77
Haynes, M. P. 1990, in Clusters of Galaxies, edited by W. R. Oegerle, M. J. Fitchett, and L. Danly (Cambridge University Press, New York), p. 177
Haynes, M. P., and Giovanelli, R. 1984, AJ, 89, 758
Haynes, M. P., and Giovanelli, R. 1986a, ApJ, 306, 466
Haynes, M. P., and Giovanelli, R. 1986b, ApJL, 306, L55
Haynes, M. P., Giovanelli, R., Starosta, B., and Magri, C. 1988, AJ, 95, 607
Haynes, M. P., Giovanelli, R., da Costa, L. N., Salzer, J., Wegner, G., Chamaraux, P., and Freudling, W. 1991, in preparation
Heisler, J., Tremaine, S., and Bahcall, J. N. 1985, ApJ, 298, 8
Huchra, J. P., and Geller, M. J. 1982, ApJ, 257, 423 (HG)
Kirshner, R. P., Oemler, Jr., A., Schechter, P. L., and Schechtman, S. A. 1981, ApJ, 248, L57
Lubin, P., Villela, T., Epstein, G., and Smoot, G. 1985, ApJL, 298, L1
Materne, J. 1978, A&A, 63, 401
Melnick, J., and Sargent, W. L. W. 1977, ApJ, 215, 401
Nilson, P. 1973, Uppsala Astr. Obs. Ann., 6, Uppsala General Catalogue of Galaxies (UGC)
Palumbo, G. G. C., Tanzella-Nitti, G., and Vettolani, G. 1983, Catalog of Radial Velocities of Galaxies (Gordon and Breach, New York)
Pierce, M. J., and Tully, R. B. 1988, ApJ, 330, 579
Puche, D., and Carignan, C. 1988, AJ, 95, 1025
Rose, J. A. 1979, ApJ, 231, 10
Sandage, A., and Tammann, G. 1988, Revised Shapley–Ames Catalog (Carnegie Institute of Washington, Washington, DC)
Schechter, P. 1976, ApJ, 203, 297
Thompson, L. A., Welker, J., and Gregory, S. A. 1979, PASP, 90, 644
Tully, R. B. 1980, ApJ, 237, 390
Tully, R. B. 1982, ApJ, 257, 389
Wegner, G., Haynes, M. P., and Giovanelli, R. 1991, in preparation
West, M. J., and Bothun, G. D. 1990, ApJ, 350, 36
Zwicky, F., Herzog, E., Karpowicz, M., Kowal, C., and Wild, P. 1961–1968, Catalogue of Galaxies and Clusters of Galaxies (California Institute of Technology, Pasadena), Vols. 1–6 (CGCG)